National Library of Canada
Acquisitions and Bibliographic Services Branch
395 Wellington Street
Ottawa, Ontario
K1A 0N4

Bibliothèque nationale du Canada
Direction des acquisitions et des services bibliographiques
395, rue Wellington
Ottawa (Ontario)
K1A 0N4

Your file Votre référence

Our file Notre référence

NOTICE

The quality of this microform is heavily dependent upon the quality of the original thesis submitted for microfilming. Every effort has been made to ensure the highest quality of reproduction possible.

If pages are missing, contact the university which granted the degree.

Some pages may have indistinct print especially if the original pages were typed with a poor typewriter ribbon or if the university sent us an inferior photocopy.

AVIS

La qualité de cette microforme dépend grandement de la qualité de la thèse soumise au microfilmage. Nous avons tout fait pour assurer une qualité supérieure de reproduction.

S'il manque des pages, veuillez communiquer avec l'université qui a conféré le grade.

La qualité d'impression de certaines pages peut laisser à désirer, surtout si les pages originales ont été dactylographiées à l'aide d'un ruban usé ou si l'université nous a fait parvenir une photocopie de qualité inférieure.

Canada

A STUDY OF THE OPERATING VARIABLES OF THE JAMESON CELL

Allen James Summers

A Thesis submitted to the Faculty of Graduate Studies and Research
in partial fulfillment of the requirements of the degree of
Master of Engineering

Dept. of Mining and Metallurgical Engineeering
McGill University
Montreal, Canada

ISBN 0-612-07985-6

Canada

ABSTRACT

The Jameson cell is a relatively new flotation device that has been successfully used in several applications, ranging from mineral recovery to de-oiling dairy effluents. The cell comprises a plunging jet bubble column (downcomer) which discharges in a separation tank. The effect of operating variables on Jameson cell performance, *e.g.*, gas holdup in the downcomer and interaction between the downcomer and separation tank, was investigated in this thesis.

Gas holdup in the downcomer of the Jameson cell was determined using conductivity measurements with ring-shaped electrodes installed in the interior wall of the downcomer. The Maxwell model was used to calculate the gas holdup from the conductivity measurements. In both two-phase and three-phase tests, the conductivity technique gave adequate estimates of the actual downcomer gas holdup. The conductivity signal was also shown to be able to detect process disturbances (*e.g.*, changes in flow regime).

Interaction between the downcomer and the separation tank was studied by altering the level in the separation tank. When gas flowrate was not controlled, the level affected the gas flowrate, pressure, pool level/free jet length, mixing zone length, and gas holdup in the downcomer. A pressure technique was used to determine the mixing zone length..

The effect of the superficial gas velocity on the froth/pulp interface position in the separation tank was also studied. Although no relationship could be drawn between gas flowrate and separation tank level, froth flooding or loss of froth interface was observed at a superficial gas rate (with respect to the separation tank) ≥ 1.2 cm/s.

RÉSUMÉ

La cellule Jameson est une nouvelle technologie de flottation, qui a eu du succès remarquable dans plusieurs applications. L'effet des variables opérantes sur la performance de la cellule Jameson a été étudié.

La fraction de gaz dans la colonne de collection (''downcomer'') a été déterminée en se servant de mesures de conductivité prises avec des électrodes annulaires installées à l'intérieur de la colonne. Le modèle Maxwell a été utilisé pour faire les calculs de fraction de gaz à partir des mesures de conductvité.

Les estimés de la fraction de gaz par méthode de conductivité furent raisonnables pour les essais binaires et ternaires. Le signal de conductivité a aussi été en mesure de detecter les perturbations de procédé.

L'interdépendance des deux composants de la cellule Jameson (colonne de collection, cellule de séparation) a été étudiée. On remarque que le niveau dans la cellule de séparation influence quelques variables opérantes de la colonne de collection, soient: le débit d'air, la pression de vide, le niveau dans la colonne, et la fraction de gaz. L'effet du niveau dans la cellule de séparation sur la largeur de la région de turbulence a été étudié en utilisant des mesures de pression à l'intérieur de la colonne.

Le débit de gaz à la cellule de séparation a eu un effet sur la présence d'une interface évidente entre la mousse et le liquide, dans la cellule de séparation. Des vélocités superficielles d'air supérieures à 1.2 cm/s ont causé la perte d'une interface de mousse.

ACKNOWLEDGEMENTS

I would like to thank the following people, whose contribution in the preparation of this work was greatly appreciated:

My supervisor, Prof. J.A. Finch, for his guidance, patience, and for his enthusiasm for my work. I have thoroughly enjoyed the opportunity to study under him.

Dr. Cesar Gomez and Dr. Manqui Xu, for their leadership and experience in the preparation of in-plant research campaigns, and experimental design.

Martin Knoepfel, Joe Boka, Michel Leroux, and Ray Langlois for their immense contribution in the building and designing of the laboratory apparatus.

Felix Palaeri, Alex Probst, Liming Huang, and the Kidd Creek concentrator personnel for their help with the in-plant test work.

Finally, I would like to thank my family and friends, whose love and support throughout this endeavour made it most gratifying.

TABLE OF CONTENTS

LIST OF FIGURES

LIST OF TABLES

NOMENCLATURE

A	Electrode cross-sectional area, (cm^2)
b	jet/column area ratio, (dimensionless)
D_J	Jet diameter, (m)
D_N	Nozzle diameter, (m)
d_m	Maximum stable bubble diameter, (m)
E	Energy dissipation rate, ($kg\ m^2\ s^{-2}$)
f	Volume fraction, (dimensionless)
h	Liquid level in separation tank, (cm)
I	Current flow, (A)
J_f	Superficial feed velocity, ($cm\ s^{-1}$)
J_g	Superficial gas velocity, ($cm\ s^{-1}$)
J_g^d	Superficial gas velocity in downcomer, ($cm\ s^{-1}$)
J_g^s	Superficial gas velocity in separation tank, ($cm\ s^{-1}$)
k	Electrolyte conductance, ($S\ cm^{-1}$)
l	Electrode path length, (cm)
L	Mixing zone length, (m)
L_j	Free jet length, (m)
P	Pressure, (Pa)
P_a	Atmospheric pressure, (Pa)
P_{bot}	Pressure at bottom of downcomer, (Pa)
P_d	Dynamic pressure of decelerating liquid jet, (Pa)
P_h	Hydrostatic pressure in downcomer, (Pa)
P_{vac}	Vacuum pressure at top of downcomer, (Pa)
Q_{air}	Volumetric air flowrate, ($l\ min^{-1}$)
Q_{feed}	Volumetric feed flowrate, ($l\ min^{-1}$)

r	radius, (m)
R	Resistance, (Ω)
V	Potential difference, (v)
We_c	Critical Weber number, (dimensionless)
z	Pool level in downcomer, (cm)

Greek Letters

ρ	Liquid density, (kg m^{-3})
ρ_{sl}	Slurry density, (kg m^{-3})
σ	Liquid surface tension, (N m^{-1})
κ	Specific conductance, (S)
κ_c	Specific conductance of continuous phase, (S)
κ_d	Specific conductance of dispersed phase, (S)
κ_m	Specific conductance of mixture, (S)
λ_1	Gas/liquid volumetric flow ratio, (dimensionless)
ε_g	Fractional gas holdup, (dimensionless)
μ_j	Jet velocity, (m s^{-1})

CHAPTER 1

INTRODUCTION

1.0 ADVENT AND APPLICATION OF THE JAMESON CELL

There have been many innovations in froth flotation within the last 10 years. Column flotation technology and its implementation in industry advanced rapidly and other flotation devices were developed as alternatives to conventional mechanical cells and columns. Among this new wave of devices is the Jameson cell. Developed jointly by Professor Graeme Jameson of the University of Newcastle, New South Wales, Australia, and Mount Isa Mines, the Jameson cell utilizes a novel method for gas introduction and bubble generation. A major advantage is that the cell requires about a third the space of a flotation column (Jameson, 1988). Since its inception, the Jameson cell has had wide interest due to its compact design. Its application to treat lead-rich slime material at the Mount Isa Mines Pb/Zn concentrator, and to make a cyanide-soluble Cu concentrate prior to gold leaching at the Red Dome Au/Cu concentrator, are examples where considerable improvement over existing technology (mechanical cells and flotation columns) was realised. concentrate (Harbort *et al.*, 1994). The Jameson cell has also found extensive use in the coal industry for the concentration of fine coal and producing a low ash content. A non-mineral application which is growing rapidly is in de-oiling of effluents from petroleum and food processing.

1.1 THE JAMESON CELL

Figure 1.1 is a schematic of the Jameson cell. It consists of two main sections: A vertical pipe section in which particle collection occurs, called the downcomer, and a cylindrical tank, called here the separation tank, in which the collected particles form a froth. The feed

under high pressure (20-40 psi) is introduced at the top of the downcomer through a nozzle or orifice plate, producing a high speed slurry jet. The jet entrains the air initially in the downcomer, and once the level of slurry in the separation tank has reached the bottom of the downcomer, a vacuum is produced by this air entrainment of the jet which lifts slurry up the downcomer, filling it to the level of the orifice plate. The Jameson cell is self aspirating, the vacuum produced by the jet draws atmospheric air through an air inlet located at the top of the downcomer at the same height as the orifice plate. The air is entrained into the jet and then sheared into fine bubbles as the jet plunges into the slurry pool in the downcomer. The upper area of the slurry pool in the downcomer is termed the mixing zone, an area of extremely turbulent flow where intense mixing occurs and particles and bubbles collide in a strong shear field are sheared together. Below this region, a uniform, dense foam region of high gas fraction (50 - 60%) develops, an area highly favourable for further particle collection. The material exits the bottom of the downcomer and enters the separation tank. Loaded bubbles rise to the top of the separation tank forming a froth zone, while the uncollected particles exit from the bottom. The froth, cleaned with the use of wash water, overflows into a concentrate launder and the uncollected particles become the tailings.

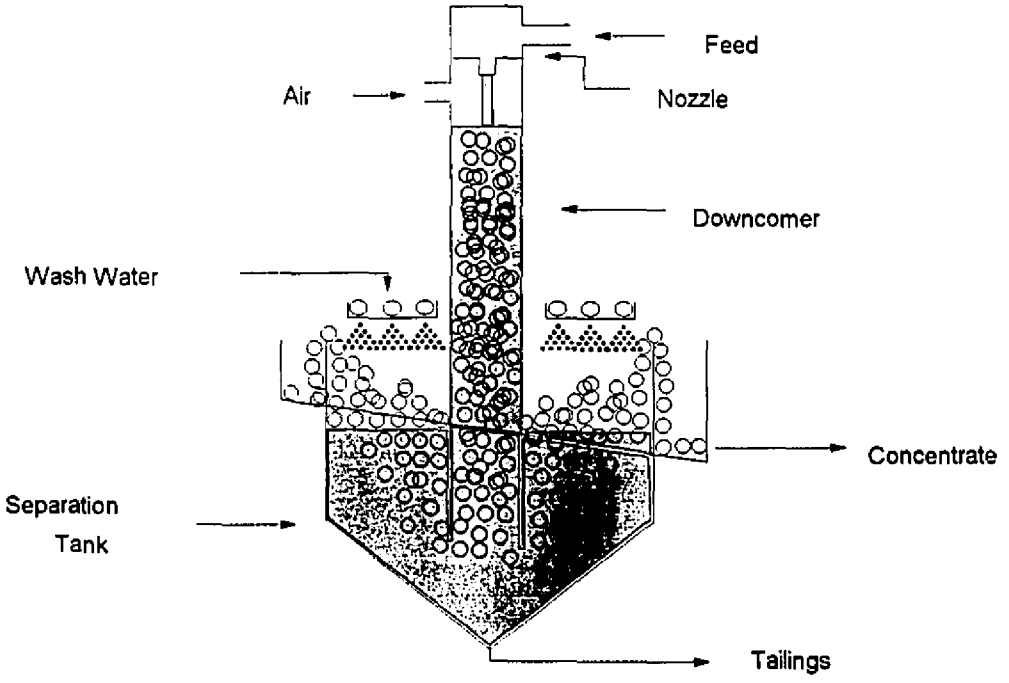

Figure 1.1: Schematic of the Jameson cell

1.2 CONTROL VARIABLES IN THE JAMESON CELL

As with the flotation column, the Jameson cell has 2 zones which appear to control metallurgical performance, a collection zone (downcomer) and a froth zone (formed in the separation tank). The downcomer is essentially a concurrent downflow bubble column, using air entrainment and bubble formation with a plunging jet. An alternative name, therefore, is a plunging jet bubble column. High gas holdup is possible in the downcomer because of the bubble buoyancy force is counteracted by the downward liquid motion. Since gas holdup is a variable which affects collection efficiency and the surface area available for particle transport, its on-line determination would help to optimize downcomer performance.

The froth zone in the separation tank of the Jameson cell behaves much like that in the flotation column. Froth depth has been shown to significantly affect column performance (Huls, Lachance, and Dobby, 1989), although this is not always the case (Espinosa-Gomez *et al.*, 1989). In the Jameson cell, grade and recovery are controlled by wash water, froth depth and superficial air velocity in the separation tank (Jameson and Manlapig, 1991).

1.3 THESIS OBJECTIVE

The use of conductance measurements to estimate process variables in flotation column, notably gas holdup and froth depth, has been documented (Uribe-Salas, 1991). It is the purpose of this thesis to investigate the applicability of similar techniques to measure process variables in the Jameson cell, in particular to gauge the interaction between the downcomer and separation tank.

1.4 THESIS OUTLINE

Chapter 2 contains a review of the hydrodynamics of the plunging jet bubble column. The operating variables of the Jameson cell are also introduced.

Chapter 3 contains basic electrical conductivity theory, and reviews the use of electrical conductance measurements to estimate process variables in flotation and other mineral processing applications.

Chapter 4 summarizes results of the use of ring electrodes to measure conductance in the Jameson cell downcomer in the estimation of gas holdup and detection of process disturbances in a laboratory Jameson cell unit. The experimental apparatus used in this research is described, as well as a review of the experimental procedures.

In Chapter 5, the interaction between the downcomer and separation tank is investigated, specifically the effect of separation tank level on downcomer performance and the effect of superficial gas flowrate and gas holdup in the downcomer on the gas holdup distribution in the separation tank.

The conclusions from the research and suggestions for future work are presented in Chapter 6.

CHAPTER 2

THEORETICAL BACKGROUND TO THE JAMESON CELL

2.0 INTRODUCTION

As explained in Chapter 1, the Jameson cell consists of two main compartments: i) the downcomer, where is where air entrainment, bubble formation, and particle-bubble contact occur, and ii) the separation tank, where the particle-laden bubbles disengage from the pulp and form a froth layer. In this chapter, both will be described and the theory of their operation detailed. Finally, the effect of several operating variables on overall cell performance is discussed.

2.1 THE PLUNGING JET BUBBLE COLUMN/JAMESON CELL DOWNCOMER

2.1.1 Hydrodynamic Zones of the Downcomer

In his study of the plunging jet bubble column (PJBC), Evans (1990) divided the column into four main hydrodynamic zones (Figure 2-1): a) The free jet zone, in which the jet properties are determined by the nozzle geometry and turbulence in the jet delivery system, b) the plunging jet zone, where air entrainment occurs at the plunge point, c) the mixing zone, in which the entrained air is sheared into bubbles and thoroughly mixed with the slurry phase, and d) the uniform two-phase (gas-slurry) flow zone, in which the dispersion flows downwards and is released into the separation chamber.

2.1.2 The Mechanism of Entrainment in the Jameson cell/PJBC

Evans (1990) considered that the rate of entrainment for a rough-surfaced plunging jet to be the sum of the quantity of gas trapped within the boundary of the jet at the point of impact with the receiving liquid, and the quantity of gas composing the annular gas film between the free surfaces of the jet and the receiving liquid at the point of impact.

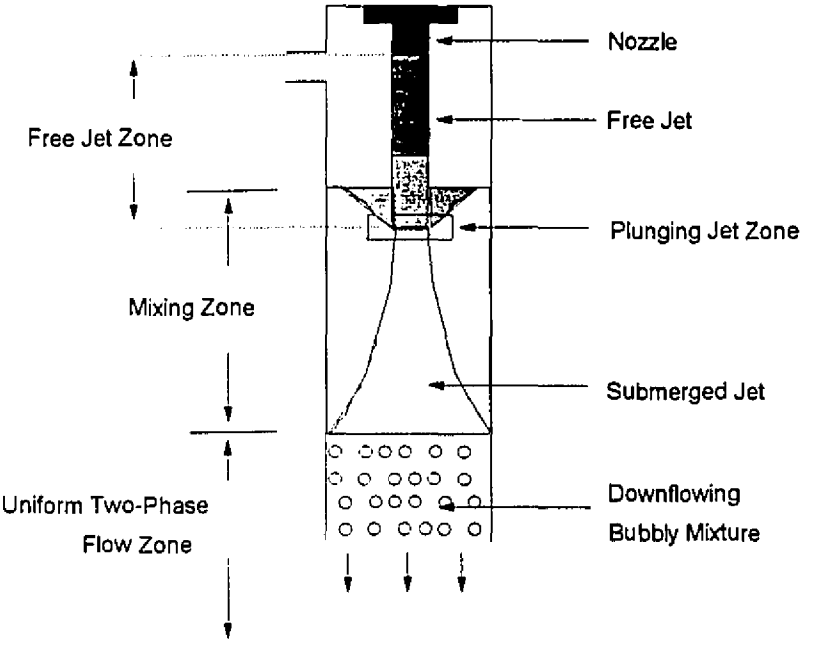

Figure 2.1 Hydrodynamic zones of a plunging jet bubble column (from Evans,1990)

The gas film component of entrainment can be calculated from determination of the film thickness. Evans showed that the film thickness could be estimated from thin film theory, assuming that the film did not rupture before it became a uniform thickness. Evans also found that gas film entrainment in smooth jets was controlled by the velocity of the recirculating eddy. The effect of the column diameter on the gas film entrainment can thus be determined by the effect the column diameter has on the recirculating eddy velocity. Evans' assumptions for gas entrainment by a confined plunging were: Entrained gas is contained within the effective diameter of the free jet at plunge point, as well as in the annular film adjacent to the surface of

the jet. The outward boundary of the film is defined as a streamline separating entrained and un-entrained components of the moving gas boundary layer (Figure 2-2).

In their development of a model to predict the rate of gas entrainment for a liquid jet plunging in a confined column of liquid, Evans *et al.* (1994) divided the free jet zone into three regions: a) Region 1, where immediately upon exiting the nozzle, the plunging slurry jet entrains air as a film adjacent to the jet surface; b) Region 2, where the jet velocity is assumed constant and waves on the jet surface form causing air to be entrained within the jet envelope, as well as in the film adjacent to the jet surface (see Figure 2-3); c) Region 3, where as the effective jet diameter increases, the diameter of the streamline reduces to zero resulting in no film, and entrainment occurs as gas trapped within the jet envelope.

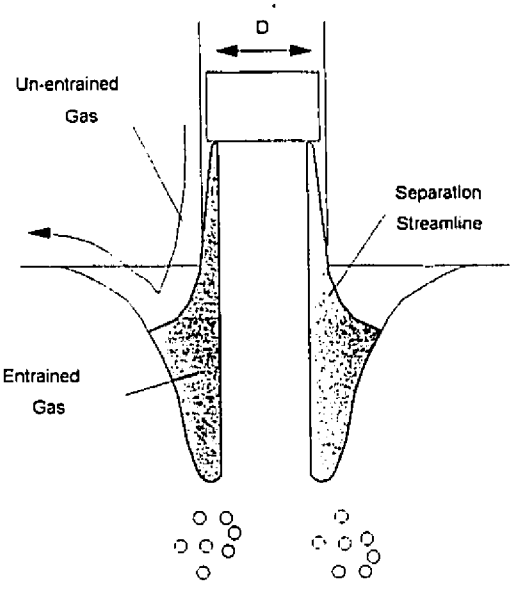

Figure 2.2 Gas entrainment model for a confined plunging liquid jet (from Evans *et al.*, 1994)

2.1.3 Mixing Zone

The following description of the mixing zone is from the findings of Evans (1990) in his work with the plunging jet bubble column (PJBC). The mixing zone in the Jameson cell/PJBC

develops as a result of the expansion of the submerged jet. Momentum of the submerged jet is diffused radially to the surrounding liquid. The momentum transfer causes the velocity of the surrounding liquid to increase while that of the liquid in the submerged jet decreases.

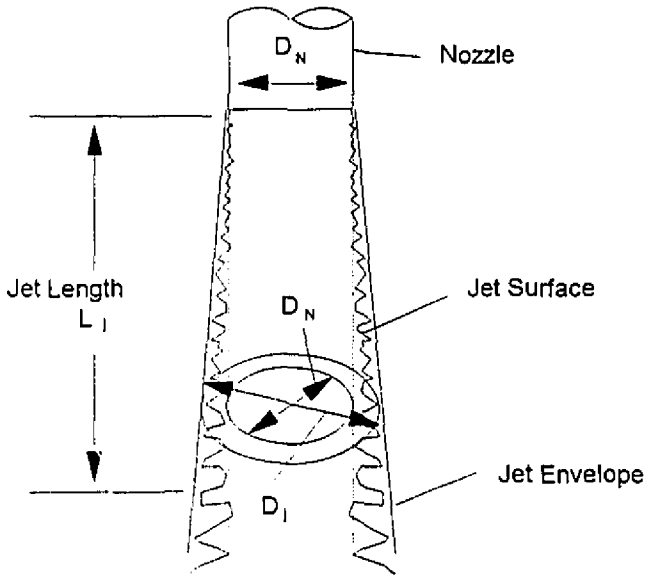

Figure 2.3 Effective jet diameter of a confined plunging liquid jet (from Evans *et al.*,1994)

The submerged jet expands to fill the downcomer, and then swirls upward, forming a loop around the surrounding liquid (Figure 2-4a). The surrounding liquid thus develops a circular motion forming recirculating eddies (Figure 2-4b). The velocity profile generated within the recirculating eddy is important for the following reasons: a) The velocity at the boundary of the eddy which forms the free surface of the induction trumpet controls the rate of film-wise entrainment, and b) the boundary velocity of the recirculating eddy influences the expansion of the submerged jet. The diameter of gas bubbles formed by the shear stresses at the boundary between the submerged jet and the surrounding liquid play an important role in defining the operation of the downcomer, *e.g.* gas holdup and the amount of recycled gas. Both gas holdup and the recycled gas component increase with increasing bubble size (increased bubble rise

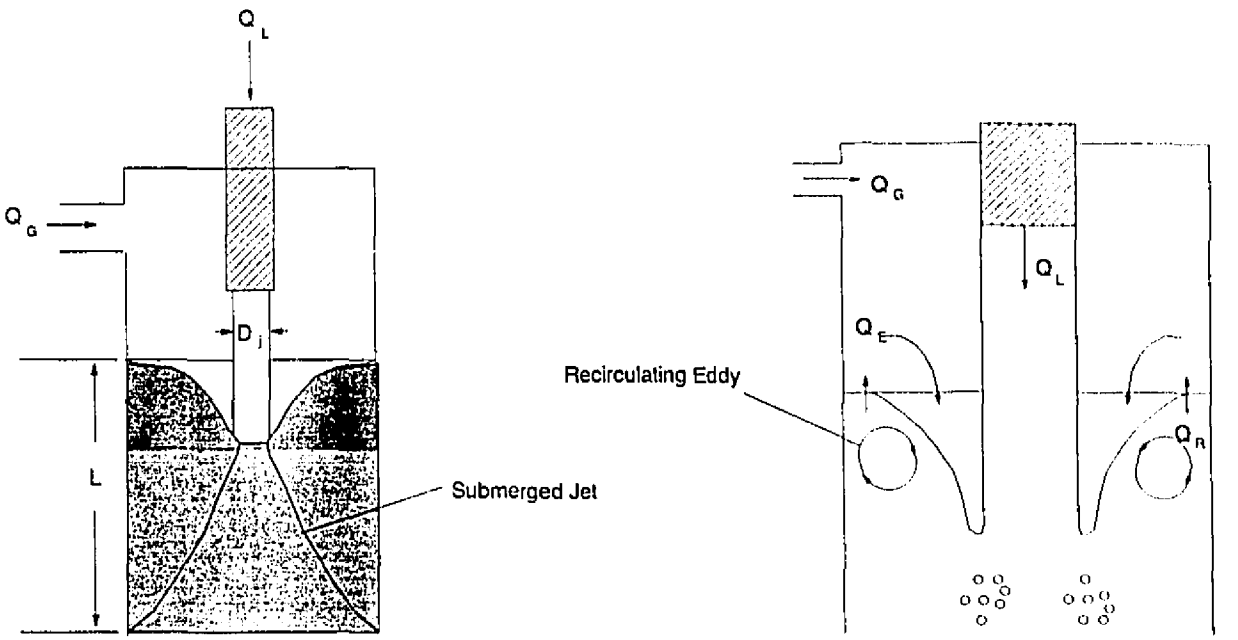

Figure 2.4 (a) Submerged jet expansion in a plunging jet bubble column (from Evans *et al.*, 1992) (b) Rate of entrainment in a confined plunging jet (from Evans *et al.*, 1994)

Evans and co-workers (1992) developed equations to determine the maximum stable bubble diameter generated in the mixing zone. Assuming that the average energy dissipation rate per unit volume experienced by the bubble is uniform throughout the mixing zone, then the maximum stable bubble diameter is:

$$d_m = \left(\frac{We_c \sigma}{2}\right)^{3/5} \rho^{-1/5} E^{-2/5} \qquad (4.1)$$

$$e_c = \frac{\rho \overline{u^2} d_m}{\sigma} \quad (4.2)$$

ρ and σ are the liquid density and surface tension, respectively, d_m is the maximum bubble diameter, $\overline{u^2}$ is the average value of the square of the velocity acting over a scale length equivalent to the maximum bubble diameter, and E is the average energy dissipation rate per unit volume experienced by the bubble. For flows where the energy dissipation rate per unit volume is not uniform throughout the field, such as in the mixing zone of a plunging jet bubble column, Evans *et al.* derived the following expression:

$$E = \frac{\rho u_j^3}{2L} [b - 2b^2 - b^3 (1 + \lambda_l)^2 + 2b^3(1 + \lambda_l)] \quad (4.3)$$

where u_j is the jet velocity, L is the mixing zone length, b is the jet/column area ratio, and λ_l is the gas/liquid volumetric flow ratio.

2.1.4. Flow Regime

Oshinowo & Charles (1974) observed the following flow regime transitions in vertical downflow systems with increasing gas flowrate (Figure 2–5): a) Bubble–coring flow, where bubbles migrate towards the axis of the column forming a core of dispersed bubbles, b) bubbly–slug flow, in which the formation of rising slugs occurs, c) falling film flow, which is characterized by the liquid flowing as a thin film along the tube wall, containing virtually no gas bubbles, with the gas core containing no liquid droplets: this type of flow occurs at low flowrates, d) falling bubbly–film flow, which is similar to falling film flow but the liquid film is thicker and contains finely dispersed air bubbles, e) froth flow, characterized by a highly turbulent mixture of large air bubbles merging with liquid, and finally f) annular flow in which

the liquid flows down as an annular film, and the gas core contains liquid droplets. In a study by Yamagiwa *et al.* (1990) the following flow regime transitions were observed, in order of increasing liquid velocity: bubble–stagnant flow, non–uniform bubbling flow, uniform bubbling flow, churn–turbulent flow, and once again uniform bubbling flow. According to Evans (1990), there are four flow regimes that can develop in the uniform two–phase flow zone (Figure 2–6): bubbly flow, slug flow, churn–turbulent flow, and annular flow. In bubbly flow, small bubbles of differing diameter travel downward with about the same velocity as the liquid phase. The smaller bubbles tend to travel along the centre axis of the column while larger bubbles accumulate along the wall of the downcomer. Bubbly flow is observed at low gas flowrates. As the gas flowrate is increased, bubbles coalesce to form large spherical cap–shaped bubbles called slugs which can span the whole diameter of the column. This flow pattern is termed slug flow. Although these large bubbles have large buoyancy forces, drag and viscous forces may act to impart a net downward motion to these slugs. At higher gas rates, the slugs grow in length and increase in velocity, until shearing forces causes the breakdown of these bubbles creating a turbulent flow of liquid and gas packets. This is termed churn–turbulent flow. At even higher gas flowrates, the liquid flows down the downcomer walls, while gas forms a core at the centre. This is termed annular flow.

2.2 THE FROTH ZONE OF THE JAMESON CELL

The froth zone in the separation tank of the Jameson cell functions similarly to the froth zone of a flotation column, in that superficial gas velocity, froth depth, and wash water affect the performance significantly.

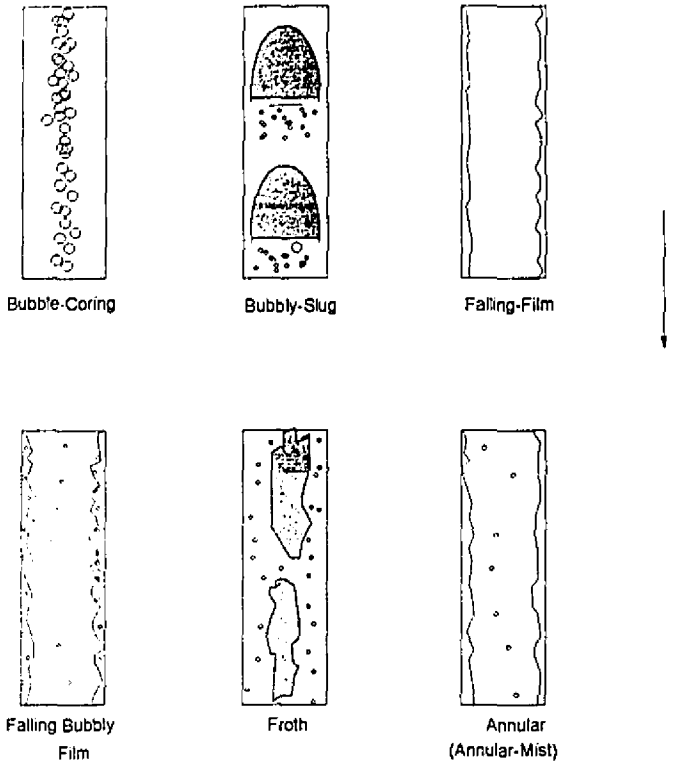

Figure 2.5 Flow patterns in vertical downflow (from Oshinowo and Charles, 1974)

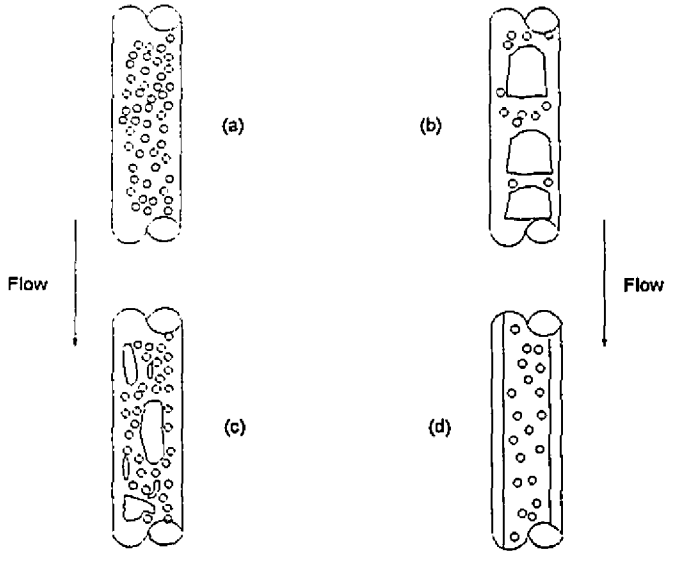

Figure 2.6 Flow regimes in a plunging jet bubble column (from Evans, 1990)

2.2.1 Gas Flowrate and Superficial Gas Velocity

In flotation columns, as the superficial gas velocity increases the concentrate grade tends to decrease due to an increase in entrainment of fine gangue. Overall recovery also increases with increased gas rate, and this can be predicted by a fundamental model of the collection zone (Finch and Dobby, 1990). Froth zone recovery has also been shown to increase with increasing gas rate(Wilson and Stratton-Crawley, 1991[as reported by Finch *et al.*, 1995]). Finch and co-workers suggest the additional gas rate helps the transport of heavy froth over the lip. The effect of superficial gas velocity in the froth zone of the Jameson cell has also been investigated (Jameson and Manlapig, 1991). By varying gas rates in the downcomer, and by using a froth crowder to vary superficial gas velocities in the separation tank, it was found that the increase in superficial gas velocity caused an increase in solids production rate and recovery (Figures 2-7 and 2-8 respectively). The use of the froth crowder alone increased recovery from 40 to 90%. Optimizing the superficial gas velocity is very important in the performance of the Jameson cell. Too high gas rates causes froth flooding, leading to the loss of the froth-pulp interface, a very dilute froth, and subsequent loss in selectivity (Atkinson *et al.*, 1993).

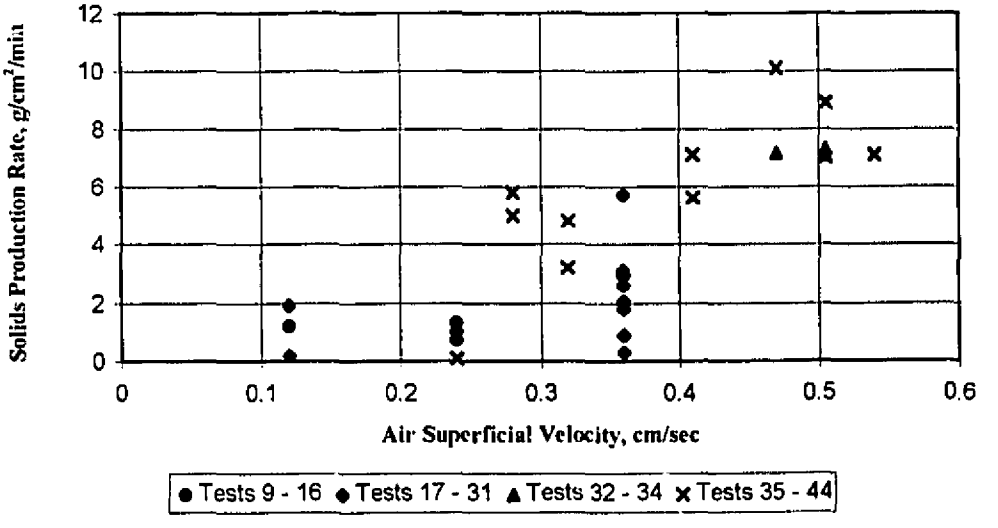

Figure 2.7 Concentrate solids production rate vs. air superficial velocity (Jameson & Manlapig,1991)

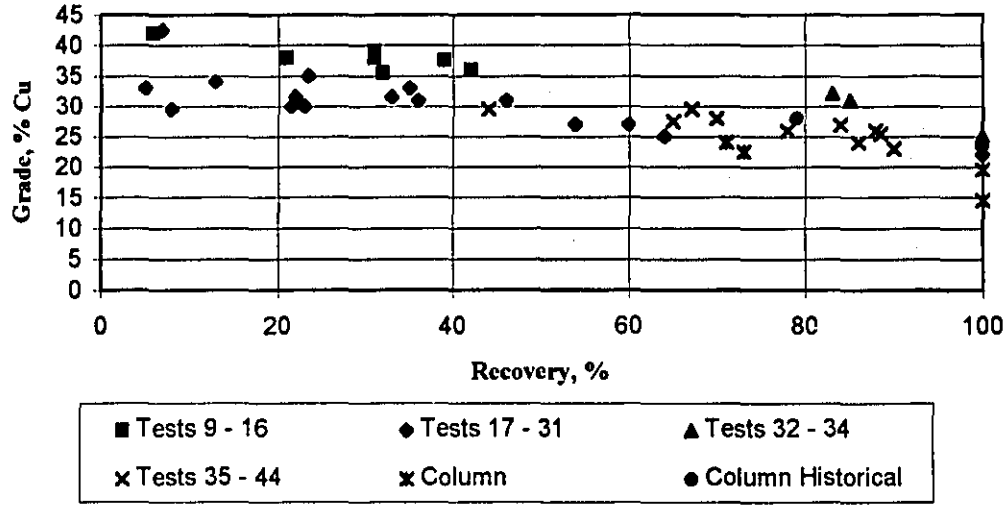

Figure 2.8 Grade vs. recovery curve; Tests 32-44 denotes highest air superficial velocity (Jameson & Manlapig, 1991)

2.2.2 Froth Depth

Froth depth can have an important effect on froth zone performance in a flotation column (Finch and Dobby, 1990). The froth depth of the Jameson cell has also been found to have a significant effect (Jameson & Manlapig, 1991; Tremblay *et al.*, 1993). Tremblay and co-workers found that the froth depth had a more significant effect on recovery than grade. Jameson and Manlapig observed a decrease in solids recovery rate with increasing froth depth (Figure 2-9).

2.2.3 Wash Water

Wash water is added at the top of flotation columns, into the froth zone, to remove fine hydraulically-entrained gangue particles. Optimum bias rates (wash water rate minus concentrate water rate) should be about zero, which corresponds to a wash water ratio (wash

water flowrate/concentrate water flowrate) of 1.0 (Finch *et al.*, 1995). Wash water addition to the froth zone of the Jameson cell has been found to work much like that in the case of the flotation columns. One study found the best grade was achieved with a wash water ratio of 1.0, *i.e.*, zero bias.

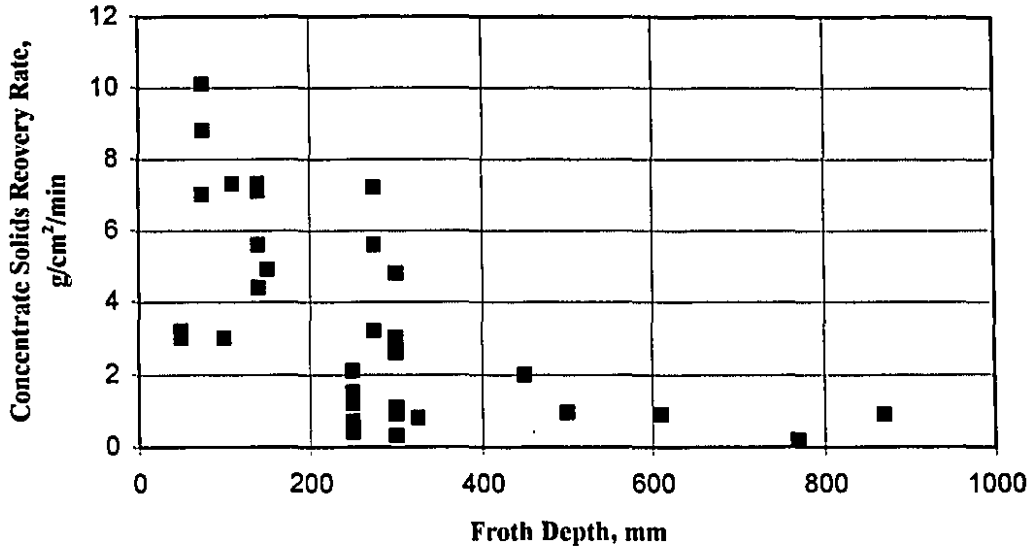

Figure 2.9 Concentrate solids production rate vs. froth depth (Jameson & Manlapig, 1991)

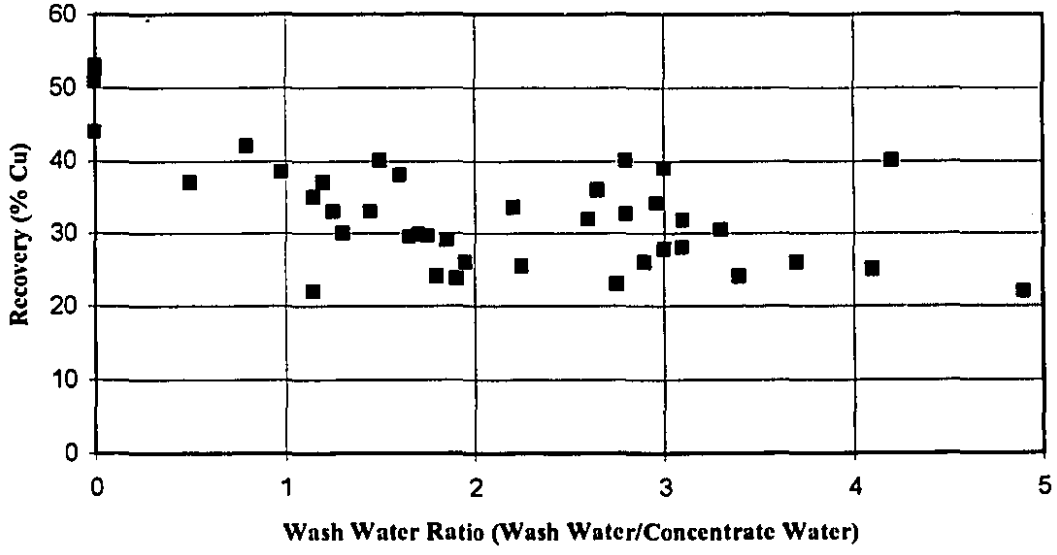

Figure 2.10 Cu recovery vs. wash water ratio (from Atkinson *et al.*,1993)

Atkinson and co-workers also found that as the wash water ratio was increased to 1 the recovery decreased significantly, and as the wash water ratio was further increased, recovery decreased more gradually (Figure 2-10). As for the grade, it was found to increase substantially as the wash water ratio approached 1, yet no grade improvement was observed as a result of further wash water (Figure 2-11). Thus it appears that, as with flotation columns, it is important to maintain the bias at or around zero.

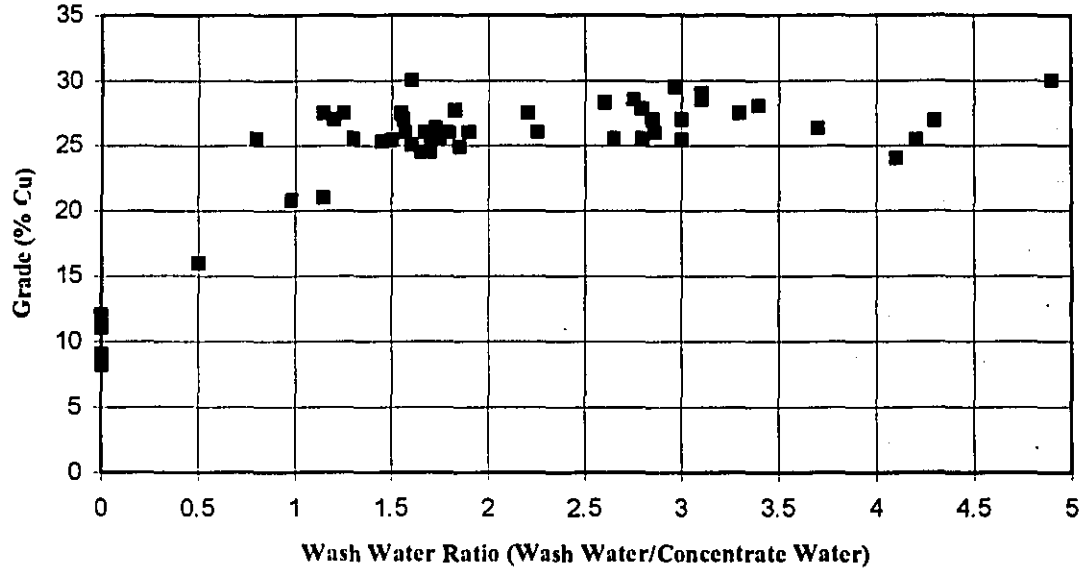

Figure 2.11 Concentrate grade vs. wash water ratio (from Atkinson *et al*, 1993)

2.3. OPERATING VARIABLES OF THE JAMESON CELL/PJBC

2.3.1 Gas Holdup in the Plunging Jet Bubble Column

As mentioned earlier, gas holdup is a variable which controls the bubble surface area available for flotation. Many design and operating variables affect gas holdup (Yamagiwa *et al.*, 1990; Marchese *et al.*, 1993). Gas holdup increases with increasing jet length and jet velocity (both due to increased gas entrainment rate), and column diameter (due to decreased

liquid velocity). Increasing the nozzle diameter has the effect of increasing the volumetric flowrate of liquid hence increasing the downward liquid superficial velocity which decreases gas holdup. Marchese and co-workers found that increasing the frother concentration causes a decrease in the gas holdup which was attributed to a decreased bubble size and concomilant reduced bubble buoyancy force. However, it was also found that overall the highest gas holdup was obtained in the presence of frother as this permitted higher gas rates. An increase in slurry density was found to increase the gas holdup in the column for the same gas rate. The reasons for this observation were attributed to increased momentum, and thus increased entrainment by the slurry jet, and increased buoyancy of the bubbles due to the higher slurry density. Banisi (1994) in a study on flotation column found that the presence of solids (*i.e.*, increased slurry density) caused a decrease in gas holdup. He attributed this to an increase in bubble swarm velocity due to wake stabilization caused by the presence of solids, increasing slurry viscosity. Whatever the mechanism, assuming the same one is at play in the Jameson cell, then the prediction would be an increase in gas holdup, as in fact observed.

2.3.2 Effect of Air-to-Slurry Ratio

The gas-to-slurry ratio is an important operational parameter as it affects the performance of both compartments of the Jameson cell. In their study, Marchese and co-workers (1993) found that the limiting gas-to-liquid ratio was about 1, although it was difficult to maintain steady operation of the downcomer at that value. This ratio also was the original target operating ratio for the Jameson cell, as it was found that the one-to-one ratio optimized the performance of the downcomer (Jameson and Manlapig, 1991). More recent experience (Atkinson *et al.*, 1993) led to the conclusion that an air-slurry ratio should 0.3-0.9. Keeping this range not only gave relatively consistent metallurgical performance but also had a stabilizing effect on overall operation by producing a more uniform and finer bubble size distribution.

liquid velocity). Increasing the nozzle diameter has the effect of increasing the volumetric flowrate of liquid hence increasing the downward liquid superficial velocity which decreases gas holdup. Marchese and co-workers found that increasing the frother concentration causes a decrease in the gas holdup which was attributed to a decreased bubble size and concomitant reduced bubble buoyancy force. However, it was also found that overall the highest gas holdup was obtained in the presence of frother as this permitted higher gas rates. An increase in slurry density was found to increase the gas holdup in the column for the same gas rate. The reasons for this observation were attributed to increased momentum, and thus increased entrainment by the slurry jet, and increased buoyancy of the bubbles due to the higher slurry density. Banisi (1994) in a study on flotation column found that the presence of solids (*i.e.*, increased slurry density) caused a decrease in gas holdup. He attributed this to an increase in bubble swarm velocity due to wake stabilization caused by the presence of solids, increasing slurry viscosity. Whatever the mechanism, assuming the same one is at play in the Jameson cell, then the prediction would be an increase in gas holdup, as in fact observed.

2.3.2 Effect of Air-to-Slurry Ratio

The gas-to-slurry ratio is an important operational parameter as it affects the performance of both compartments of the Jameson cell. In their study, Marchese and co-workers (1993) found that the limiting gas-to-liquid ratio was about 1, although it was difficult to maintain steady operation of the downcomer at that value. This ratio also was the original target operating ratio for the Jameson cell, as it was found that the one-to-one ratio optimized the performance of the downcomer (Jameson and Manlapig, 1991). More recent experience (Atkinson *et al.*, 1993) led to the conclusion that an air-slurry ratio should 0.3-0.9. Keeping this range not only gave relatively consistent metallurgical performance but also had a stabilizing effect on overall operation by producing a more uniform and finer bubble size distribution.

2.3.3 Frother Addition

It has been found (Marchese *et al.*, 1993; Tremblay *et al.*, 1993) that the volume of aspirated air for a certain feed flowrate could be increased by increasing frother concentration. The air flowrate attainable would then reach a maximum at a certain frother dosage. On the other hand, a minimum amount of frother was found necessary to prevent coalescence and obtain a stable flow in the downcomer. Atkinson and co-workers (1993) found that an excess or build-up of frother led to a reduction in the maximum superficial gas velocity attainable in the Jameson cell. This then led to froth flooding due to the finer size of bubbles produced by the excessive frother concentration.

CHAPTER 3

ELECTRICAL CONDUCTANCE AND IT USE IN PROBING TWO AND THREE PHASE SYSTEMS

3.0 INTRODUCTION

Electrical conductivity measurements have been used in the study of hydrodynamics for the past century, becoming particularily prevalent in recent years (Achwal and Stepanek, 1976; Turner, 1976; Begovich and Watson, 1978; Blok and Drinkenburg, 1982; Tsochatizidis *et al.*, 1992; Marchese *et al.*, 1992; Xu *et al.*, 1993; Uribe-Salas *et al.*, 1992). The purpose of this chapter is to overview electrical conductivity and the theoretical background of electrical conductance measurements in aqueous electrolytes, and to review recent work regarding the use of electrical conductance measurements as a tool in the study of hydrodynamics of various systems.

3.1 ELECTRICAL CONDUCTIVITY

3.1.1 Definition of Electrical Conductivity

The electrical conductance of a substance depends on the potential difference to produce a certain current flow. The relationship between potential difference, current flow, and resistance, is commonly known as Ohm's law, *i.e.*,

$$v = I \bullet R \qquad 3.1$$

where V is the potential difference, with units of volts, **v**, I is the current flow, with units of amps, **A**, and R is the electrical resistance, measured in ohms, Ω. Alternately, the relationship between current and potential difference can be stated as:

$$v = \frac{I}{C} \qquad 3.2$$

where C is the electrical conductance of the material. The electrical conductance in fact is the inverse of resistance, giving rise to the unit ohm^{-1}, or mho. In the SI system, this unit is the siemens, S. Metals such as gold, silver, and copper, have a high electrical conductance because of the availability of low-energy unfilled orbitals, causing a high mobility of electrons. Electrical conductance in an aqueous electrolyte depends of the mobility of ions, not electrons. Ionic motion is imparted by a potential difference applied by two electrodes immersed in the electrolyte, with the negative ions being attracted to the anode and the positive ions attracted to the cathode. Thus current flows in the electrolyte due to the movement of ions.

3.1.2 Measurement of Electrical Conductance

The electrical conductance of an electrolyte is measured by determining the current flow when a potential difference is applied between two electrodes immersed in the electrolyte. The electrical conductivity, or the specific conductance of the electrolyte, κ, is the conductance of the electrolyte measured by a cell of unit cross-sectional area and length. When using a cell without unit dimensions, the conductivity of an electrolyte is the measured conductance multiplied by cell geometry factor, or cell constant, *i.e.,*

$$\kappa = k \bullet \frac{l}{A} \qquad 3.3$$

where l is the distance between the electrodes, A is the cross-sectional area of the electrodes, and k is conductance of the electrolyte measured by the electrode pair or cell.

3.2 PHENOMENA ASSOCIATED WITH ELECTROLYTIC PROCESSES

Unfortunately, taking conductance measurements is not as simple as the notion of immersing two metal electrodes and applying a potential implies. There are complex electrochemical reactions that are consequential to the applied voltage (Cole and Coles, 1964; Braunstein and Robbins, 1971). Some of these reactions cause further voltage drop and thus erroneous measurement of conductance.

3.2.1 Double Layer Capacitance

As each electrode attracts its oppositely charged ion, a double layer is formed by the charged pair. The electrode and oppositely charged ions adjacent to it form a capacitor capable of storing charge. When a sufficiently low voltage is applied to the electrodes, the current flow functions only to charge the capacitor.

3.2.2 Electrolysis

Because of the double layer capacitance, increased voltage is required to keep current flowing in the circuit. As the electric potential is increased beyond a critical value, decomposition of certain constituent ions of the electrolyte occurs, with oxidation reactions occurring at the anode and reduction at the anode.

3.2.3 Ohmic Resistance

As ions travel through the electrolyte, they experience drag and friction forces opposite to the accelerating effect of the electric field force. This resistance causes energy loss to take place in the form of heat.

3.2.4 Concentration Polarization

As the voltage is further increased, the decomposition of the electroactive ions (ions oxidisable and reducible in the range of the voltage applied) may occur faster than the diffusion of such species from the bulk electrolyte to the electrode surface. The concentration gradient produced causes the current flow to be limited by the rate of diffusion.

3.2.5 The Role of Alternating Current

Voltage reversal, by the substitution of a direct current (DC) voltage source by an alternating current (AC) voltage source, imparts a reversal of direction of travel to the ions. As the frequency of the voltage reversal is increased, concentration polarization can be reduced or eliminated. Decomposition can be averted by using a reduced applied AC voltage and using reversible electrodes.

3.3 EFFECT OF ELECTRODE SHAPE ON CONDUCTANCE MEASUREMENTS

Kasper (1940) found that there are three cases in which uniform current flow exists between electrodes: i) Infinite parallel planes, ii) concentric cylinders of infinite length, and iii) concentric spheres.

3.3.1 Infinite Parallel Plates

The following assumptions are made: The anode and the cathode are equipotential surfaces, that the lines of current flow leave perpendicular to the anode, intersect a series of equipotential surfaces and strike the cathode at a normal; the electrolyte is electrically isotropic and homogeneous; a constant current flows between the electrodes; and the current density of the electrodes is constant.

The case of infinite parallel plates is analogous to a linear conductor. The resistance of the system is:

$$R = \frac{\Delta V}{I} = \frac{V_A - V_B}{I} \qquad 3.4$$

In the case of the linear conductor where the current density on the equipotential surface is constant, then:

$$i = -\kappa \frac{\delta V}{\delta x} = \frac{I}{A} \qquad 3.5$$

Integrating the above yields :

$$R = \frac{l}{\kappa A} \qquad 3.6$$

where l is the length of conductor. Rewriting the equation gives the relationship between conductivity and conductance.

$$\kappa = \frac{K l}{A} \qquad 3.7$$

3.3.2 Two Concentric Cylinders of Infinite Length

Given two concentric cylinders, the smaller one with radius R_1, and the larger cylinder with radius r_2, the lines of current flow linking the equipotential surfaces are radii, normal to both cylinders and are drawn from the central axis of both cylinders. The current density is assumed to be uniform over the equipotential surface of the cylinders; then:

$$i = -\kappa \frac{\partial V}{\partial x} = \frac{I}{2\pi r} \qquad 3.8$$

Integrating the above yields:

$$_1 - V_2 = \frac{I}{2\pi\kappa} \ln\frac{r_1}{r_2} \qquad 3.9$$

The resistance per unit length therefore becomes:

$$R = \frac{2.303}{2\pi\kappa} \log\frac{r_1}{r_2} \qquad 3.10$$

Radial sectioning of the system yields equivalent systems.

3.3.3 The Flow Between Two Concentric Spheres

Given two concentric spheres, the smaller inner sphere of radius r_1, and the larger sphere of radius r_2, the lines of current extend radially from the center of both spheres. The current density over both spherical surfaces is:

$$i = -\kappa \frac{\partial V}{\partial r} = \frac{I}{4\pi r^2} \qquad 3.11$$

Integration yields:

$$_1 - V_2 = \frac{I}{4\pi\kappa}\left(\frac{1}{r_1} - \frac{1}{r_2}\right) \qquad 3.12$$

Therefore the resistance of the system is:

$$R = \frac{1}{4\pi\kappa}\left(\frac{1}{r_1} - \frac{1}{r_2}\right) \qquad 3.13$$

and as $r_2 \rightarrow \infty$, $1/r_2$ goes to 0. Therefore the resistance of the system is almost entirely dependant on the size of the outer sphere when the radius of the larger sphere is much greater than that of the smaller sphere.

3.4. ELECTRICAL CONDUCTIVITY OF DISPERSIONS

The electrical conductivity of dispersions has been a topic of research over the past century, and has been reviewed in several publications (De la Rue and Tobias, 1959; Banisi *et al.*, 1993) The focus of this review will be the use of models to determine the volume fraction of non-conducting dispersed phase (*i.e.,* air bubbles) from the conductivity of the dispersion.

3.4.1 The Maxwell Model

For a dilute (volume fraction $f \leq 0.2$) random suspension of uniform spherical particles of conductivity κ_d, in a continuous medium of conductivity κ_c, Maxwell(1892) determined the following relationship between the dispersion conductivity and the conductivities of the components, and the volume fraction of each:

$$K_m = \frac{2\kappa_d + \kappa_c + f(\kappa_d - \kappa_c)}{2\kappa_d + \kappa_c - 2f(\kappa_d - \kappa_c)}\,\kappa_c \qquad 3.14$$

When the conductivity of the dispersed phase is zero *e.g.,* air bubbles, the above equation reduces to:

$$K_m = \frac{(1-f)}{(1+2f)}\,\kappa_c \qquad 3.15$$

3.4.2 The Bruggeman Model

As an extension to Maxwell's model, Bruggeman (as reviewed by Banisi *et al.*, and De La Rue and Tobias) developed a model taking into account the effect of neighbouring particles in the dispersion. He arguedthat if there is a large spherical particle in a dispersion consisting of much smaller particles, the effect of the smaller particles on the electrical field around the larger particle is negligible. The larger particles can thus be considered as part of the continuum and follow Maxwell's model. Bruggeman's analysis led to the following model:

$$1 - f = \frac{\kappa_m - \kappa_d}{\kappa_c - \kappa_d}\sqrt[3]{\frac{\kappa_c}{\kappa_m}} \qquad 3.16$$

and for non-conducting dispersed phase the Bruggeman model reduces to:

$$1 - f = \left(\frac{\kappa_m}{\kappa_c}\right)^{2/3} \qquad 3.17$$

The Bruggeman model is valid only for a wide size range and dilute concentration of dispersed phase.

3.4.3 The Fricke Model

Fricke (1925), as reviewed by Banisi *et al.*, proposed a model to take into account the shape of the dispersed particles. In the case of an oblate spheroid, with half axes a, b, and c, where a≠b=c, Fricke derived the following equation:

$$\left(\frac{\kappa_m - \kappa_c}{\kappa_d - \kappa_m}\right)\left(\frac{\kappa_d}{\kappa_c} - 1\right) = \frac{\beta f}{1 - f} \qquad 3.18$$

Where:

$$\beta = \frac{1}{3}\left[\frac{2}{1 + (\frac{\kappa_d}{\kappa_c} - 1)\frac{1}{2}W} + \frac{1}{1 + (\frac{\kappa_d}{\kappa_c} - 1)(1 - W)}\right](\frac{\kappa_d}{\kappa_c} - 1) \qquad 3.19$$

and

$$(a < b) = \frac{(\varphi - \frac{1}{2}\sin 2\varphi)}{\sin^3\varphi}\cos\varphi, \quad \cos\varphi = \frac{a}{b} \qquad 3.20$$

$$(a > b) = \frac{1}{\sin^2\varphi'} - \frac{1}{2}\frac{\cos^2\varphi'}{\sin^3\varphi'}\log(\frac{1 + \sin\varphi'}{1 - \sin\varphi'}), \quad \cos\varphi' = \frac{b}{a} \qquad 3.21$$

Rearranging Fricke's equation to obtain an expression analogous to that of Maxwell:

$$\frac{(\frac{\kappa_m}{\kappa_c}) - 1}{(\frac{\kappa_m}{\kappa_c}) + x} = f\frac{(\frac{\kappa_d}{\kappa_c}) - 1}{(\frac{\kappa_d}{\kappa_c}) + x} \qquad 3.22$$

where

$$x = \frac{(\frac{\kappa_d}{\kappa_c} - 1) - (\frac{\kappa_d}{\kappa_c})\beta}{(\frac{\kappa_d}{\kappa_c} - 1) - \beta} \qquad 3.23$$

Thus for spherical particles where a=b=c, x will equal 2, and Fricke's equation reduces to Maxwell's. Then again, it is restricted in principle to dilute dispersions.

3.5 THE USE OF ELECTRICAL CONDUCTANCE MEASUREMENTS IN MINERAL PROCESSING SYSTEMS

Marchese and co-workers (1992), using a "grid" electrode geometry to make conductance measurements in the downcomer of a Jameson-type cell, found Maxwell's model to give reasonable estimates of gas holdup in two-phase and three-phase experiments as high as 60%. Marchese (1991) found that amongst several models, Maxwell's model provided the best estimates over the range of gas holdups encountered. Overestimation of gas holdup by Maxwell's model for gas holdups greater than 50% was considered to be due to changes in geometry of bubble packing, a similar argument advanced by Yianatos (Yianatos *et al.*, 1985). Indeed, Marchese found the Yianatos *et al.* model gave improved estimates of gas holdups in the range over 50%. This is significant because typical operating gas holdups in the downcomer of the Jameson cell are in the range of 50-60%. Marchese *et al.*'s finding showed potential for on-line measurement of gas holdup in the downcomer in the Jameson Cell, and thus particle collection. Atkinson and Chartiar (1992) found that the use of a portable hand-held conductivity probe to take readings of the gas/liquid mixture discharging from the downcomer was sensitive enough to detect changes in gas-to-liquid flow ratio and gas holdup in the downcomer. It has been reported that a hand-held conductivity probe can also be used to determine the froth depth in the separation tank of the Jameson cell, as alternative methods often fail (Finch, 1993). Probst *et al.* (1992) found that a measured conductance profile in the separation tank of the Jameson Cell could not precisely determine the froth depth. This was possibly due to the dynamics of the system and/or the lag time of the electronics being too long to detect a distinct interface. Xu *et al.* (1993) have used a multi-ring electrode conductivity probe to infer the mud line of a thickener from the changes in conductivity signal caused by changes in local solids concentration.

CHAPTER 4

ESTIMATION OF GAS HOLDUP AND IDENTIFICATION OF PROCESS DISTURBANCES IN THE JAMESON CELL DOWNCOMER

4.0 INTRODUCTION

Marchese (1992) found that conductivity measured with grid-shaped electrodes in the Jameson cell, in conjunction with Maxwell's model (1892), gave acceptable estimates of gas holdup. However, the "grid" electrode design was not amenable to industrial use. Testing of a non-contacting electrode, such as a ring flush-mounted in the wall, was conducted to investigate the applicability of this design to measurements of conductance in the Jameson cell.

4.1 EXPERIMENTAL APPARATUS

4.1.1 McGill Laboratory Work

The laboratory plunging jet bubble column (this term is used as opposed to Jameson cell to emphasize the generic nature of the study) consisted of a 1.81 m long, 3.81 cm ID Plexiglas downcomer (Figure 4.1). The downcomer had three flanged sections, bolted together at two Whitey stainless steel ball valves. Each valve had a 3.81 cm diameter opening, and was opened/closed by an air actuator (Whitey model MS-135-SR). A solenoid valve (ASCO model 8211C34) was used to release 100 psi of pressure to the actuators, using a compressed air cylinder combined with a pressure regulator as an air source. The two valves were used to instantaneously (response time about 150 ms) cut a sample of the middle section of the downcomer.

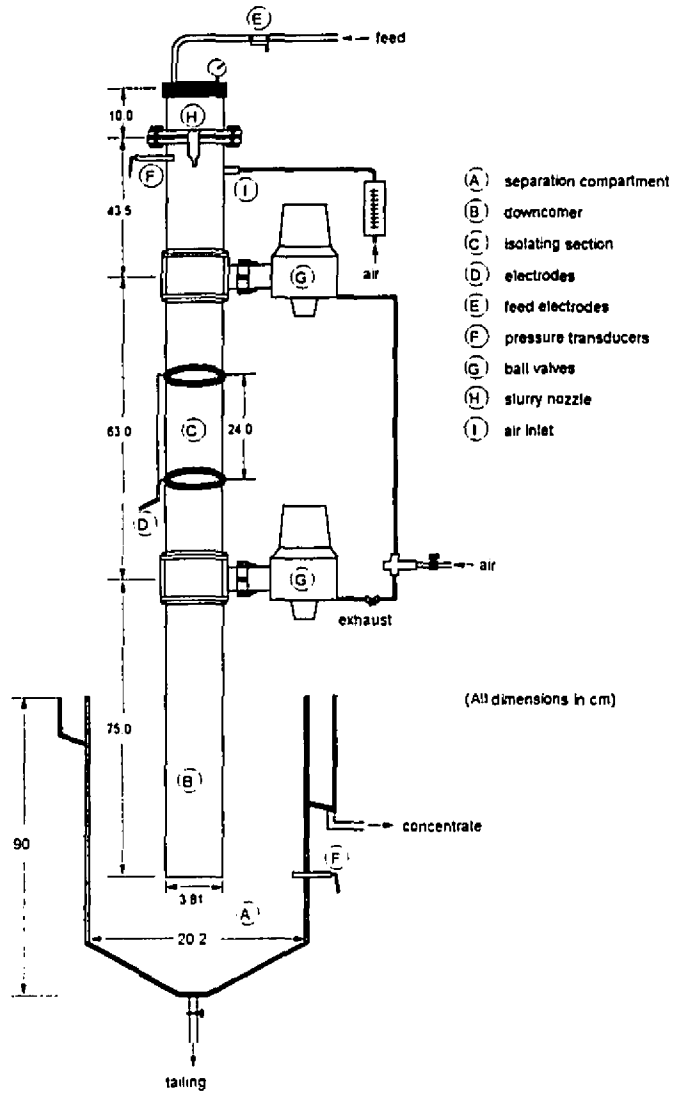

Figure 4.1 Schematic of the laboratory Jameson cell

The separation tank, also made of Plexiglas, was cylindrical, 90 cm deep with a 20.32 cm ID. A conical Plexiglas insert was made for the bottom of the tank in order to facilitate discharge of slurry and avoid any solids build-up on the bottom. The insert tapered down to a 1.905 cm discharge opening. An overflow launder was also installed on the top of the separation tank in order to collect the overflow. The nozzle assembly allowed for the ability to change the nozzle and diameter with relative ease. A 5 mm ID brass nozzle was used during the experiments.

The column was fed by two (Cole Palmer Masterflex, model 720-33) peristaltic pumps connected in parallel via a bypass valve. The bypass valve recirculated the feed back to the head tank in the closed position and its purpose was for manual measurement of the feed flowrate, as well as for diverting the feed when the downcomer ball valves were closed. A third Masterflex pump was used to control the tailings flow On-line electronic sensors on the PJBC consisted of two pressure transducers and two sets of conductance electrodes. One pressure transducer was located 2 cm below the top flange of the downcomer, and was used to measure the vacuum pressure inside the column (Omega, model PX304-05A5V). The second transducer (Druck, model PDCR860) was located at the level of the bottom of the downcomer, screwed into a fitting on the wall of the separation tank, and was used to measure the head pressure above the end of the downcomer. Air was aspirated through an orifice located 5 cm below the top flange of the downcomer. Air flow was regulated with a rotameter/needle valve assembly (Cole-Palmer, model N044-40).

Two conductance cells were used in the experiments: One to measure the conductance of the feed material, prior to being injected into the downcomer, and a second cell used to measure the conductance of the gas/liquid dispersion in the downcomer. The feed cell consisted of two stainless steel ring electrodes, 2.54 cm in diameter, 5 mm wide and approximately 1 mm thick. The electrodes were embedded 10 cm apart in a 15 cm long, 2.54 cm ID Plexiglas tube. The downcomer electrodes also consisted of two stainless steel electrodes, 3.81 cm ID, 5 mm wide and 1 mm thick. The cell electrodes were flush-mounted on the interior wall of the downcomer, 24 cm apart in the middle section of the downcomer (between the two ball valves). The location of the downcomer conductance cell was determined with the assumption that it was not in the mixing zone.

The pressure transducer and conductance cell signals were sent to an analog-to-digital signal converter interface board (Metrabyte, model DAS8-PGA). The conductance measurements were made with a conductivity meter (Tacussel, model CDRV62). A relay board (Omega model ERA-1) was used to switch between the two conductance signals, and was driven by a I/O interface board (Metrabyte model, PPA-06). An IBM-compatible microcomputer, with the aid of a program written in QuickBASIC, was used for data acquisition and relay switching. The program allowed for simultaneous trending of the

conductance and pressure measurements, and then stored the data on the hard disk once the experiment was completed.

4.1.2 Kidd Creek In-Plant Work

The laboratory plunging jet bubble column was brought to Falconbridge's Kidd Creek concentrator in Timmins, Ontario, in order to test the conductance electrodes under plant conditions. A dismountable support for the column was built prior to the campaign, which ensured stability of the apparatus while keeping it vertical, and facilitated transport .

Three test streams were chosen for the work: i) The secondary copper rougher feed, ii) the zinc primary rougher feed, and iii) the final tail.

For i) and ii), slurry was siphoned from each stream's conditioning tank. The siphon consisted of 2.54 cm steel piping, with a water hose attachment to create the suction in the siphon. A mesh screen was attached to the feed end of siphon to prevent any coarse particles or debris plugging up the piping. The siphoned slurry was fed to a 60 gallon mixing/aeration tank. A mixer was used to keep the particles in suspension. The two Masterflex feed pumps, also equipped with a mesh screen at the inlet, were used to draw the material from the mixing tank. The tailings was controlled with a pinch valve and the tailings and separation tank overflow were sent back to the flotation circuit.

The final tails material was pumped directly from the last cell in the Zn scavenger bank with the Masterflex pumps. Underflow from the laboratory column was controlled with a pinch valve and sent back to the circuit. The remainder of the experimental set-up remained the same as in the McGill laboratory experiments.

4.2 DESCRIPTION OF EXPERIMENTS

Two stainless steel rings were mounted flush with the interior wall of the laboratory Jameson cell in order to take conductance measurements of the slurry/liquid in the downcomer. A similar cell was used for conductance measurements in the feed line. The cell constants of

both electrode pairs were determined by passing KCl solutions through the cells and recording the conductance measurements with the data acquisition system. The conductivity of the KCl solutions was determined with a hand-held conductivity meter. The cell constant of the downcomer cell and of the feed cell were found to be 0.29 cm^2/cm, and 0.49 cm^2/cm, respectively. These cell constants were then entered into the data acquisition program to give direct calculation of conductivity.

Testing of the ring electrodes was conducted in two parts. First, two-phase (water-air) experiments were performed in the laboratory at McGill University. Variables such as gas flowrate, feed flowrate, frother concentration, and feed conductivity, were varied to cover a wide range of conditions. Second, testing was performed at the Kidd Creek concentrator. The feed and air flowrates were manipulated in order to vary the conditions in the Jameson cell.

In both parts, the experimental procedure was as follows: Feed was pumped into the Jameson cell, with the air line valve closed to prevent feed from entering it. The data acquisition computer program was initialized and the downcomer conductivity signal was monitored. As all of the air initially in the downcomer is driven out, the conductivity signal rises to a steady value (Figure 4.2). After readings of this steady conductivity were taken for about two minutes, from t=2.5 to t=4.5 minutes on Figure 4.2, the air line valve was opened and the air rate was set using the rotameter. As air is introduced into the downcomer at t= 4.5 minutes, the conductivity signal in the downcomer immediately dropped to a new steady-state value. The top pressure transducer shows a corresponding increase in signal (decrease in vacuum) as air is admitted into the downcomer. The height of the pool in the downcomer was measured in order to determine the downcomer gas holdup from pressure measurements. The slurry/froth was allowed to overflow freely in the separation tank in order to avoid any level effects on the pressure measurements. The new steady-state conditions were maintained for a few minutes and readings of conductivity and pressure were taken for determining the gas holdup . The downcomer ball valves were then closed and the feed to the Jameson cell bypassed in order to measure the actual gas holdup with the isolating technique. The gas holdup in the isolated section was determined using a height/volume calibration. The height of liquid/slurry was measured at the end of each test and the corresponding gas holdup was then calculated

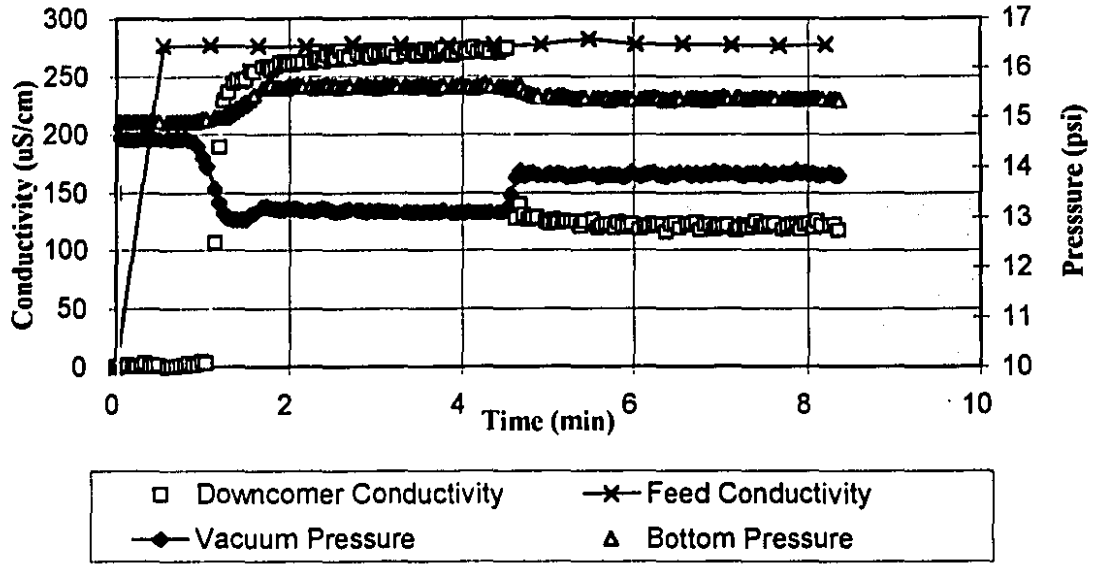

Figure 4.2 Pressure and conductivity signals taken during a test

. The data file for the experiment was saved on the computer hard disk, after which the ball valves in the downcomer were opened, allowing the material to discharge into the separation tank. The system was then ready for another test.

4.3 EXPERIMENTAL TECHNIQUES

4.3.1 Gas Holdup Determination

4.3.1.1 Isolating Technique

The isolating technique (Jepsen and Ralph, 1969) allows for a reliable measurement of average gas holdup. The two ball valves in the downcomer are closed simultaneously, while at the same time that the feed bypass valve is opened. The gas holdup in the downcomer is determined by measuring the liquid height in the isolated section. A correlation between the liquid height and liquid volume allows immediate calculation of gas holdup in the isolated section. This is taken as the actual gas holdup

4.3.1.2 Pressure Measurement Technique

The average gas holdup in a bubble column can be determined by taking pressure measurements between two points. Given pressure tappings A and B on the bubble column, the static pressure at tap A is:

$$P_A = [\rho_{sl}(1 - \varepsilon_{g,A}) + \rho_b \varepsilon_{g,A}] g L_A \quad 4.1$$

and similarly at tap B:

$$P_B = [\rho_{sl}(1 - \varepsilon_{g,B}) + \rho_b \varepsilon_{g,B}] g L_B \quad 4-2$$

where ρ_l is the slurry density, ρ_b is the bubble-aggregate density, $\varepsilon_{g,A}$ and $\varepsilon_{g,B}$ are the gas holdups above points A and B, respectively, L_A and L_B are of the position of each pressure tapping, and g is the gravitational constant. By combing the two equations, the gas holdup between the pressure taps A and B can be written as:

$$\varepsilon_g = \frac{\rho_{sl} g \Delta L - \Delta P}{(\rho_{sl} - \rho_b) g \Delta L} \quad 4.3$$

Apart from measurements taken at the tappings, all that needs to be measured is slurry density in order to determine gas holdup (Slurry density, however, may be a difficult measurement to obtain). In water-air systems, the equation reduces to:

$$\varepsilon_g = 1 - \frac{\Delta P}{\rho_{H_2O} g \Delta L} \quad 4.4$$

4.4 EXPERIMENTAL RESULTS

4.4.1 McGill Laboratory Work

Figure 4.3 summarizes data for tests using room temperature tap water (conductivity about 270 uS/cm) dosed with 5 ppm Dowfroth 250C. The superficial gas velocity in the downcomer was varied from 2-18 cm/s, while the downcomer superficial feed velocity was varied from 7-24 cm/s. As seen from Figure 4.3, in which the gas holdup determined from conductivity is plotted against the gas holdup determined directly from the isolating technique, the data is scattered. Figure 4.4 which shows the relationship of the gas holdup from pressure measurements against gas holdup determined from the isolating technique, during the same experiments as Figure 4.3. Again there is wide scatter, with a general under-estimation of the gas holdup from pressure measurements. The scatter in both sets of data may be due to bubble coalescence resulting from insufficient frother.

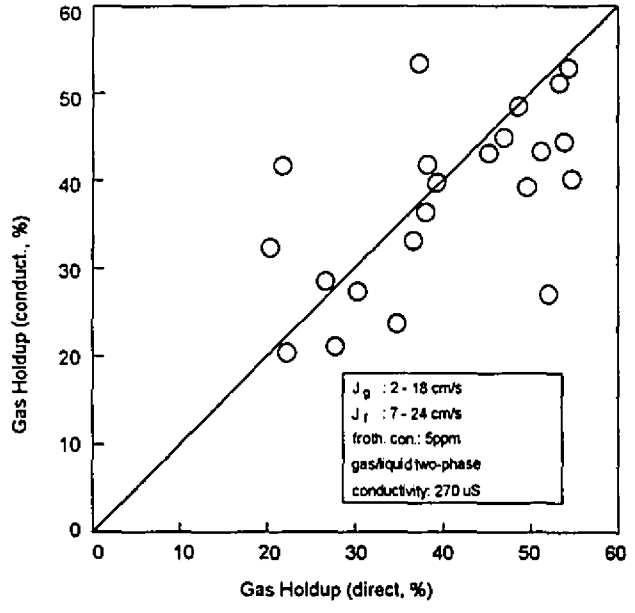

Figure 4. 3 Gas holdup from conductivity measurements versus gas holdup from direct measurements, using a 5 ppm frother dosage

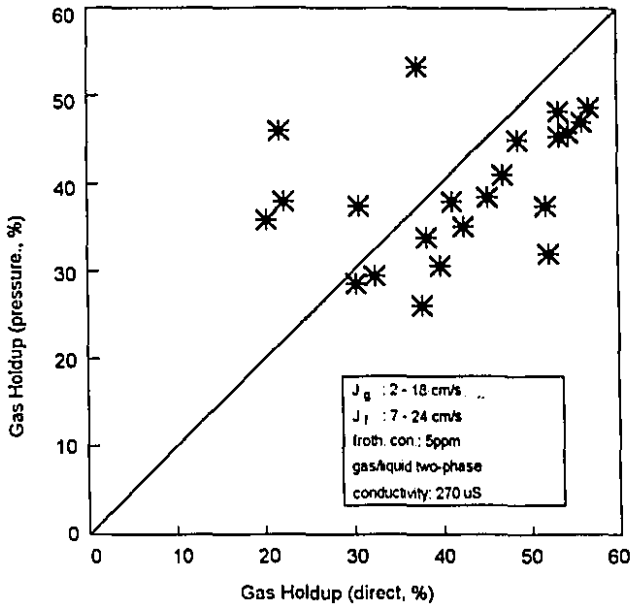

Figure 4. 4 Gas holdup from pressure measurements versus gas holdup from direct measurements, using a 5 ppm frother dosage

The 5 ppm experiments were repeated with 10 ppm and 20 ppm frother, using the same range of flow conditions (Figures 4.5 to 4.8). There is less scatter to the data and there is reasonable agreement between the gas holdup determined from the pressure and conductivity techniques with the actual gas holdup, although those from conductivity tend to be low.

Further experiments were conducted with the same range of flow conditions but with solutions of different conductivity. Potassium chloride (KCl) was added to tap water (10 ppm frother, original conductivity ≅ 230 μS/cm) to change the conductivity of the feed solution to 1000 and 2000 uS/cm. The results show that the conductivity of solution has no effect on the accuracy of the gas holdup estimation from the conductivity technique (Figure 4.9) or when using pressure (Figure 4.10).

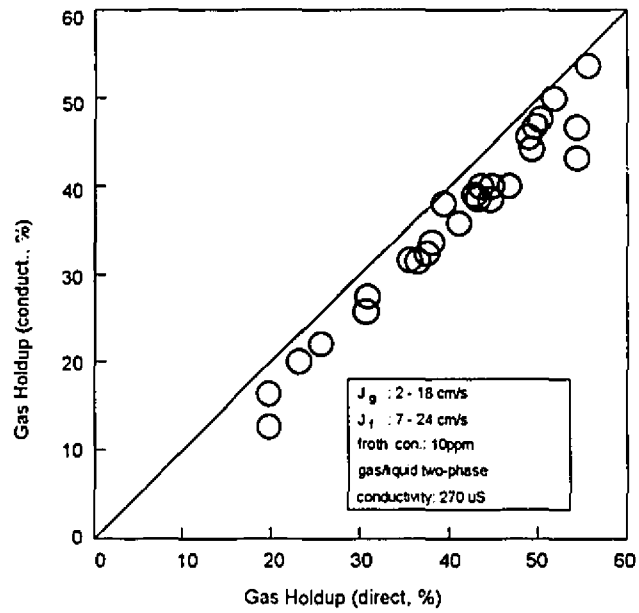

Figure 4.5 Gas holdup from conductivity measurements versus gas holdup from direct measurements, using a 10 ppm frother dosage

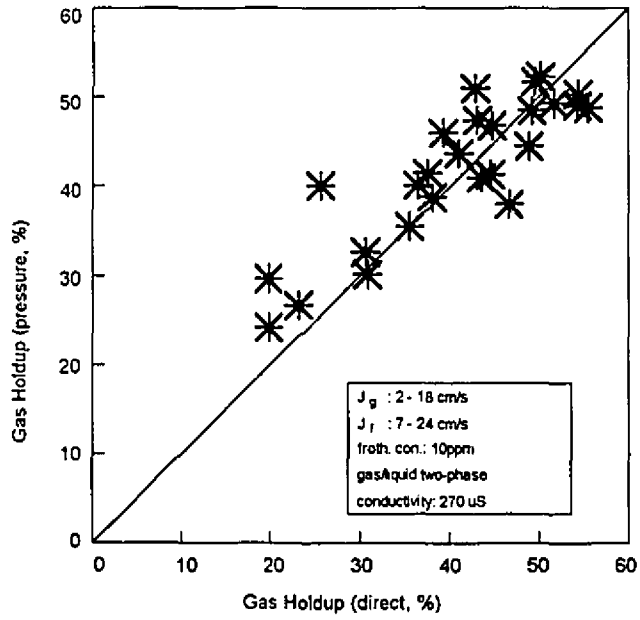

Figure 4.6 Gas holdup from pressure measurements versus gas holdup from direct measurements, using a 10 ppm frother dosage

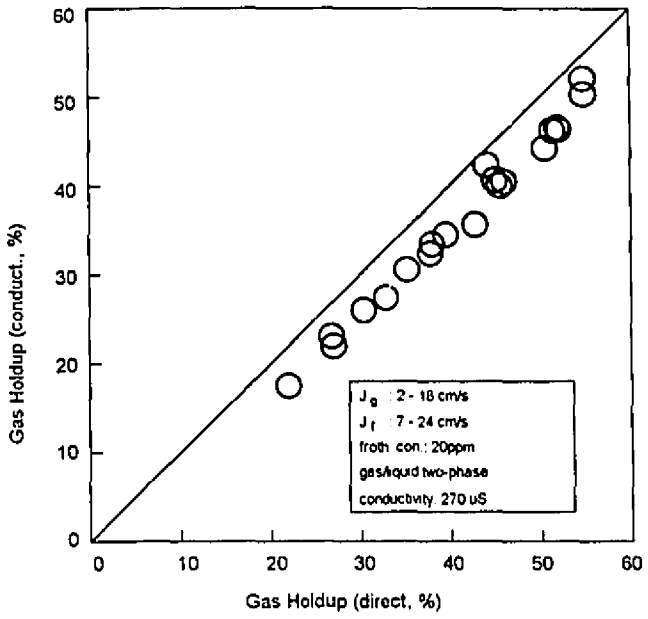

Figure 4.7 Gas holdup from conductivity measurements versus gas holdup from direct measurements, using a 20 ppm frother dosage

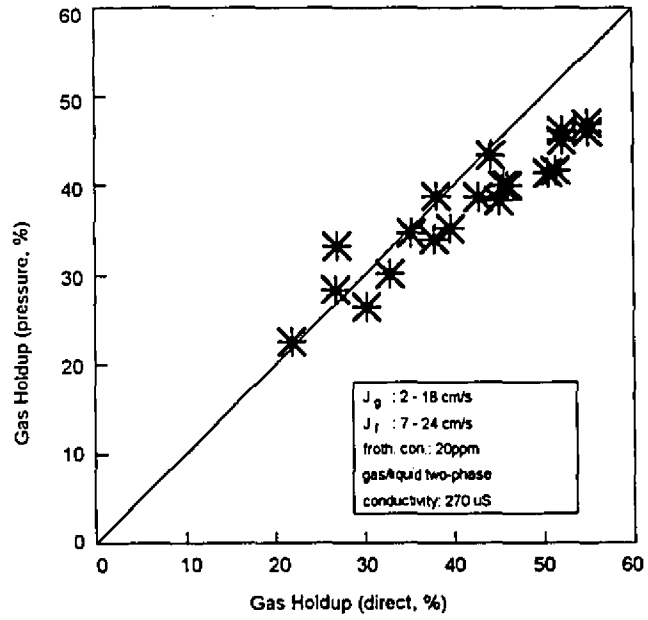

Figure 4. 8 Gas holdup from pressure measurements versus gas holdup from direct measurements, using a 20 ppm frother dosage

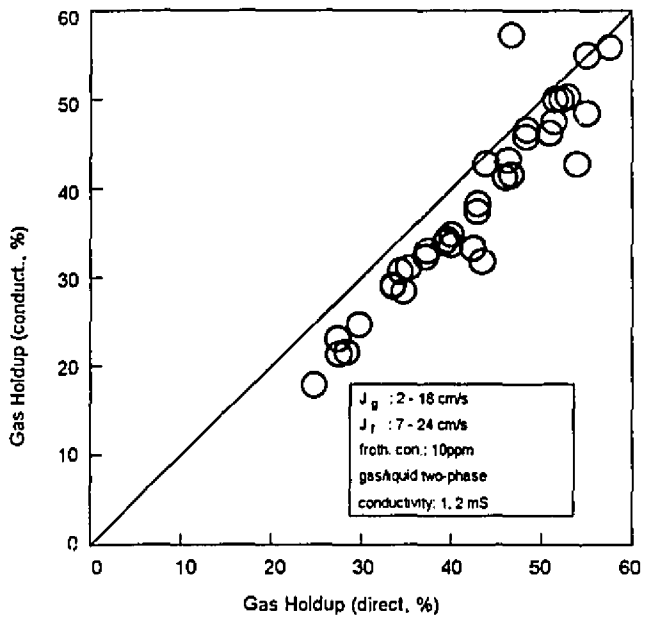

Figure 4.9 Gas holdup from conductivity measurements versus gas holdup from direct measurements, using a10 ppm frother dosage, and water conductivity of 1000 and 2000 μS/cm.

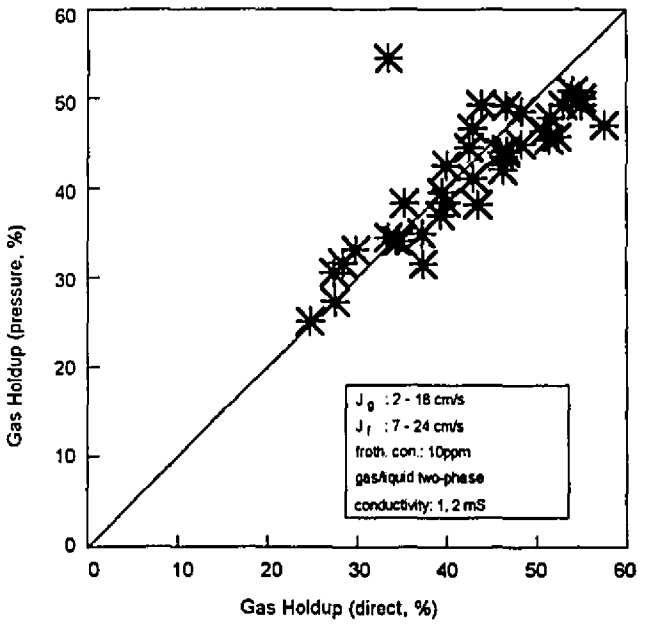

Figure 4.10 Gas holdup from pressure measurements versus gas holdup from direct measurements, using a 10 ppm frother dosage, and water conductivity of 1000 and 2000 μS/cm.

The conductivity signal from the downcomer cell can also be used to detect slug flow conditions, (which cause deterioration in performance). As shown in Figure 4.11, there is little variation in the pressure and conductivity signals during normal operation. As a slug forms and passes through the downcomer (as confirmed visually), there is a large drop in the conductivity signal (Figure 4.12), but not in the downcomer (vacuum) pressure signal. Figure 4.13, by considering signal variation, clearly shows as a slug forms and passes through the downcomer.

Figure 4.14 confirms the findings of Evans (Evans, 1990) and Marchese (Marchese, 1993), that the gas holdup in the Jameson cell downcomer is a function of the gas-to-liquid flow ratio, regardless of frother concentration.

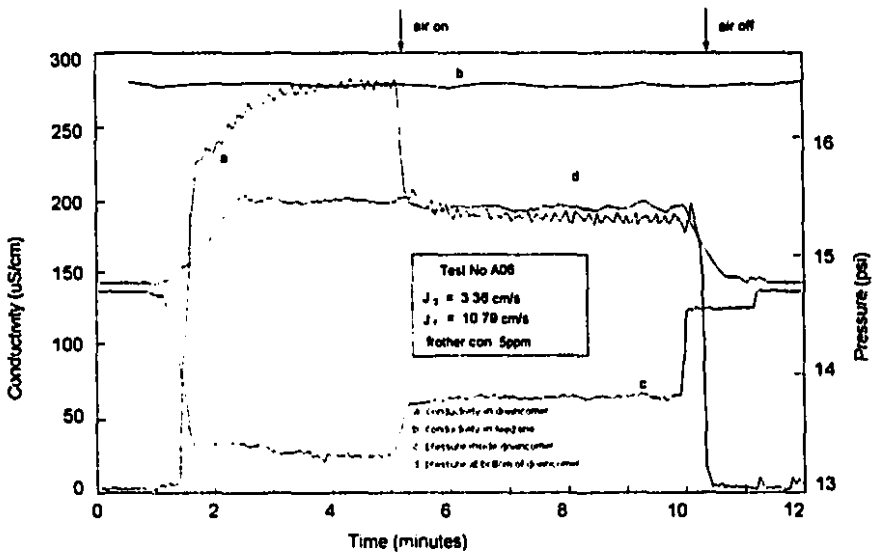

Figure 4. 11 Pressure and conductivity signals taken during a test in a bubbly flow regime

The conductivity signal from the downcomer cell can also be used to detect slug flow conditions, (which cause deterioration in performance). As shown in Figure 4.11, there is little variation in the pressure and conductivity signals during normal operation. As a slug forms and passes through the downcomer (as confirmed visually), there is a large drop in the conductivity signal (Figure 4.12), but not in the downcomer (vacuum) pressure signal. Figure 4.13, by considering signal variation, clearly shows as a slug forms and passes through the downcomer.

Figure 4.14 confirms the findings of Evans (Evans, 1990) and Marchese (Marchese, 1993), that the gas holdup in the Jameson cell downcomer is a function of the gas-to-liquid flow ratio, regardless of frother concentration.

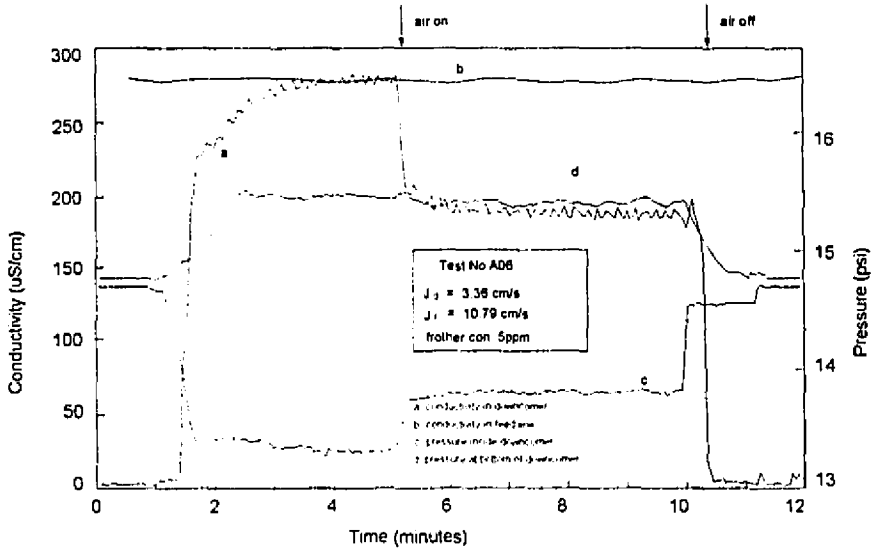

Figure 4. 11 Pressure and conductivity signals taken during a test in a bubbly flow regime

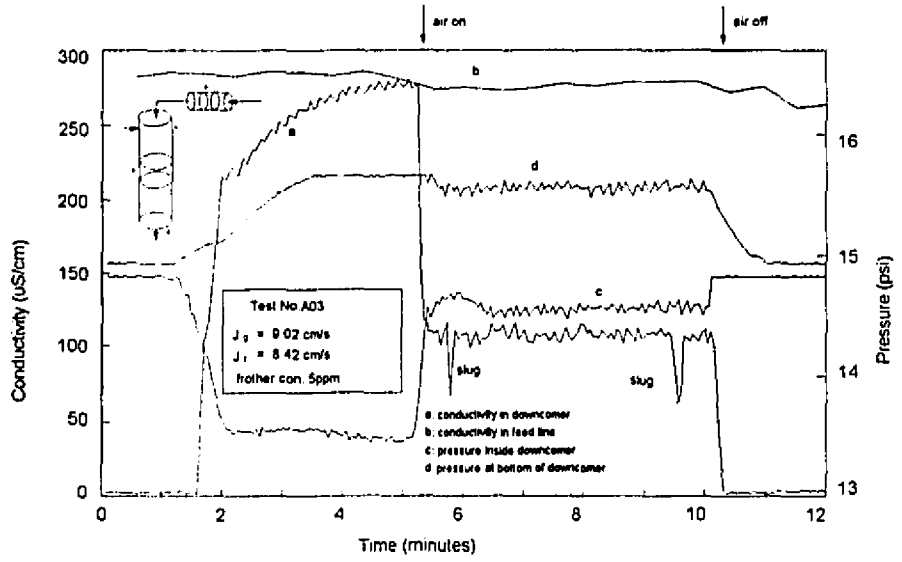

Figure 4.12 Pressure and conductivity signals taken during a test in which two slugs passed through the downcomer cell

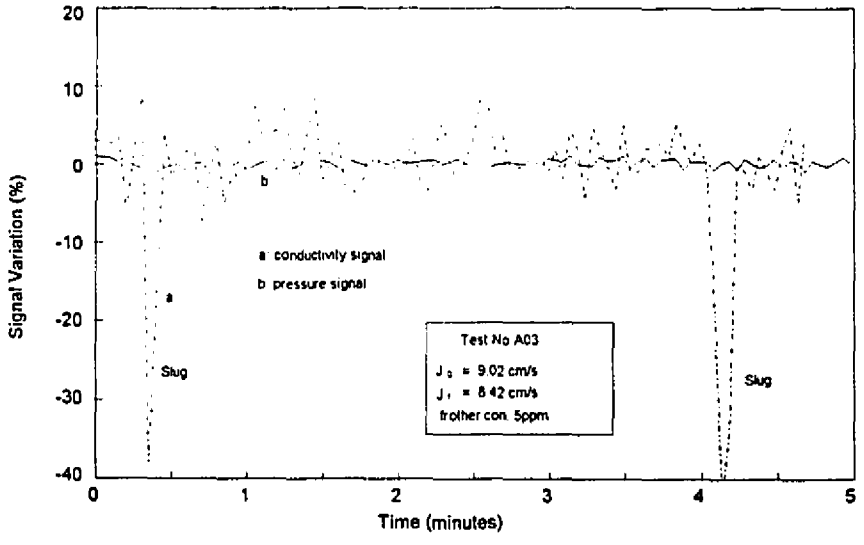

Figure 4.13 Pressure and conductivity signal variation during a test in which two slugs passed through the downcomer cell.

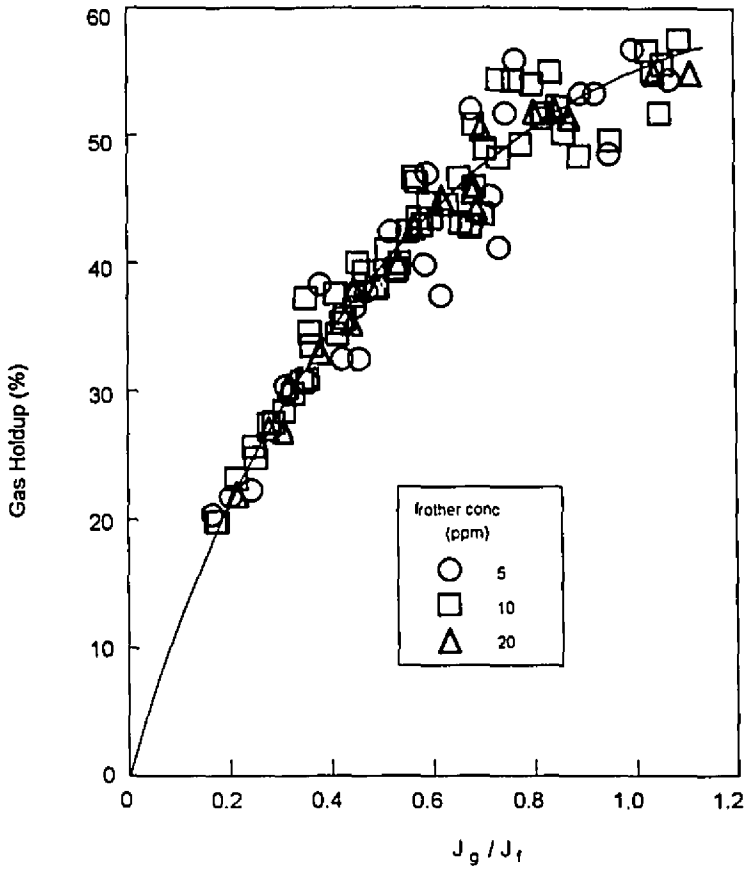

Figure 4. 14 Gas holdup in the downcomer as a function of the J_g/J_f ratio

4.4.2 Kidd Creek Work

4.4.2.1 Secondary Cu Rougher Feed

Figure 4.15 shows data from a test using the secondary copper rougher feed. The conductivity of the feed was about 2250 uS/cm. In the experiments the gas superficial velocity was varied from 0.5 to 12.5 cm/s, while the feed superficial velocity was varied from 7.5 to 19.5 cm/s. Figure 4.16 presents the gas holdup determined from the conductance measurements versus the direct measurement of gas holdup. There is scatter of data at higher gas holdups (> 45% holdup), but there is general agreement with direct measurements.

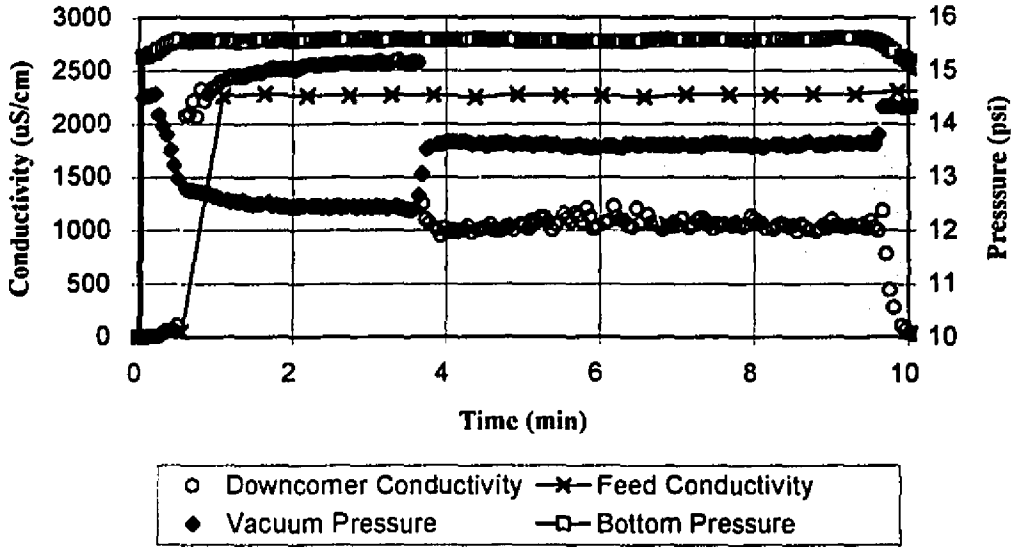

Figure 4.15 Signals taken using Kidd Creek secondary copper rougher feed stream

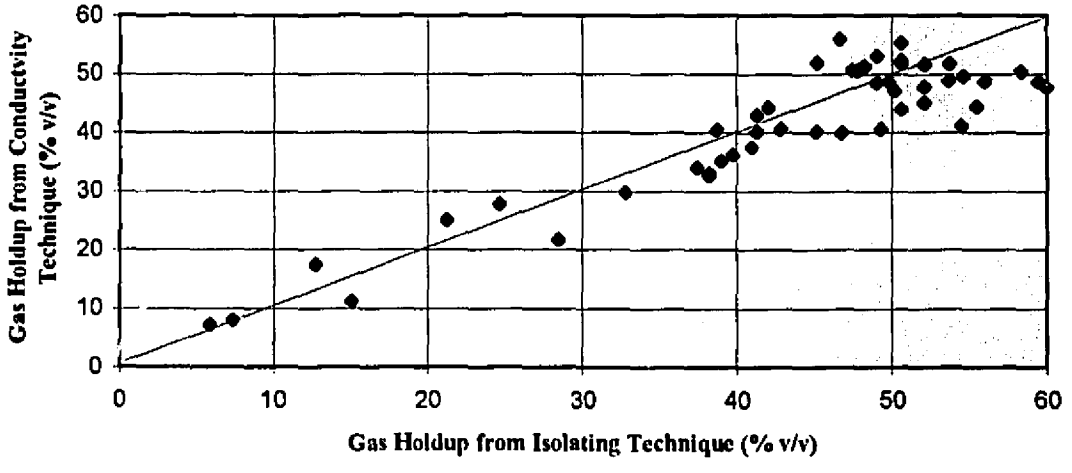

Figure 4.16 Gas holdup from conductivity measurement vs. gas holdup from direct measurement using Kidd Creek secondary copper rougher feed stream

4.4.2.2 Zn Primary Rougher Feed

Figure 4.17 is data taken during tests with the zinc primary rougher feed. The conductivity of the feed material is shown to be ≈ 225 uS/cm. The feed rate was varied from 11-18 cm/s while the gas rate was varied from 0.9-6.9 cm/s. As seen in Figure 4.18, there is good correlation between the gas holdup determined from the conductivity technique and the gas holdup determined from direct measurements. Compared to Figure 4.16, there is less scatter occurring at high holdups but a general over-estimation of the low gas holdups.

4.4.2.3 Final Tail

Figure 4.19 displays data taken during a test using the final tail as feed material. The conductivity was found to be ≈ 240 uS/cm. The superficial gas velocity was varied from 0.5 to 4.2 cm/s while the superficial feed velocity ranged from 9.5 to 18 cm/s. There was little scatter between the two gas holdup measurements (Figure 4.20); however, the maximum gas holdups in these experiments was only about 45%.

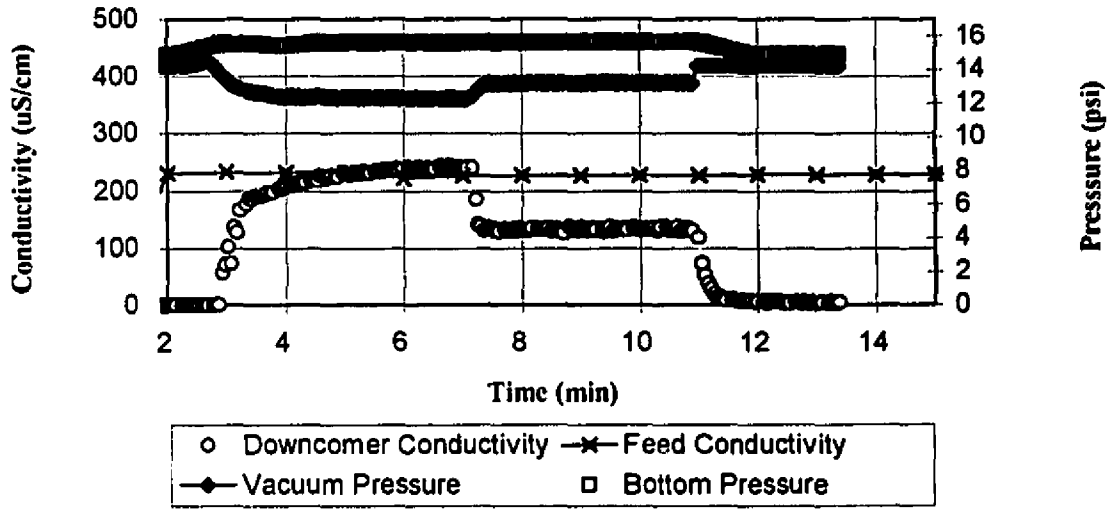

Figure 4.17 Signals taken using Kidd Creek zinc primary rougher feed stream

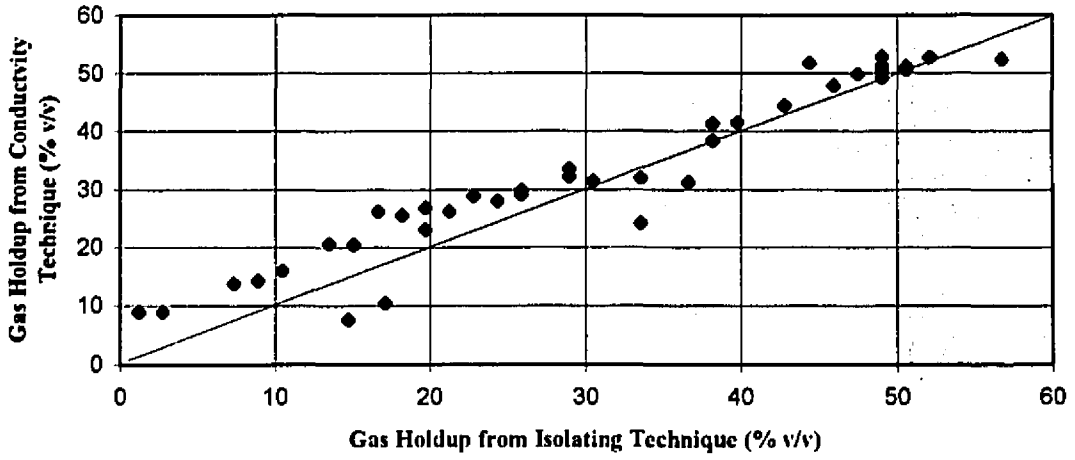

Figure 4.18 Gas holdup from conductivity measurement vs. gas holdup from direct measurement using Kidd Creek zinc primary rougher feed stream

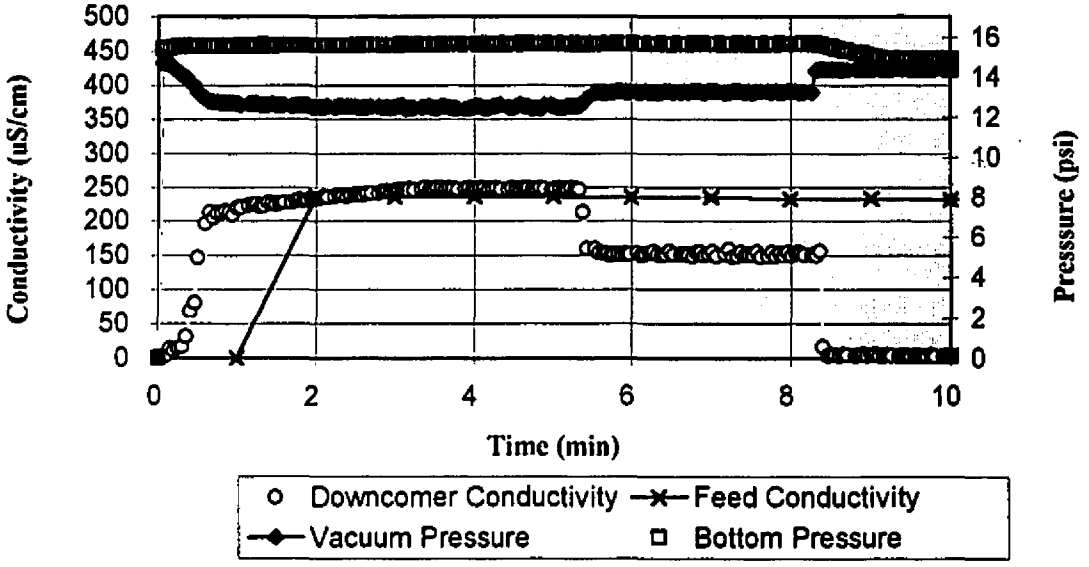

Figure 4.19 Signals taken using Kidd Creek final tail stream

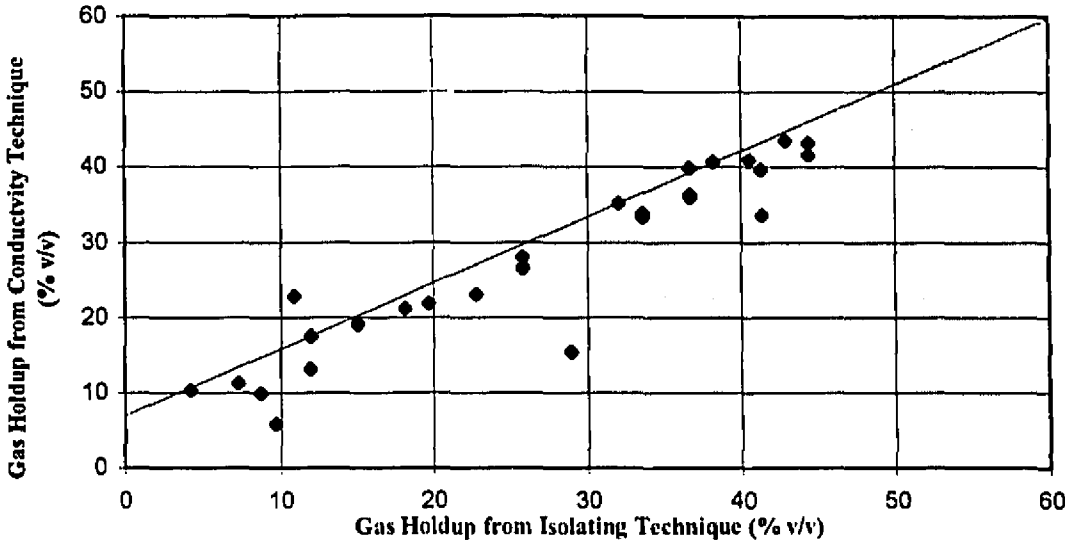

Figure 4.20 Gas holdup from conductivity measurement vs. gas holdup from direct measurement using Kidd Creek final tail stream

4.4.2.4 Flow Regime Recognition

During the test work at Kidd Creek there was further evidence that the conductivity measurements in the downcomer could be useful in the detection of slug flow. Figures 4.21 and 4.22 show tests in which the gas flow rate was sufficiently high to cause the onset of slug flow. In both cases the conductivity signal dropped immediately as the slugs passed through the cell.

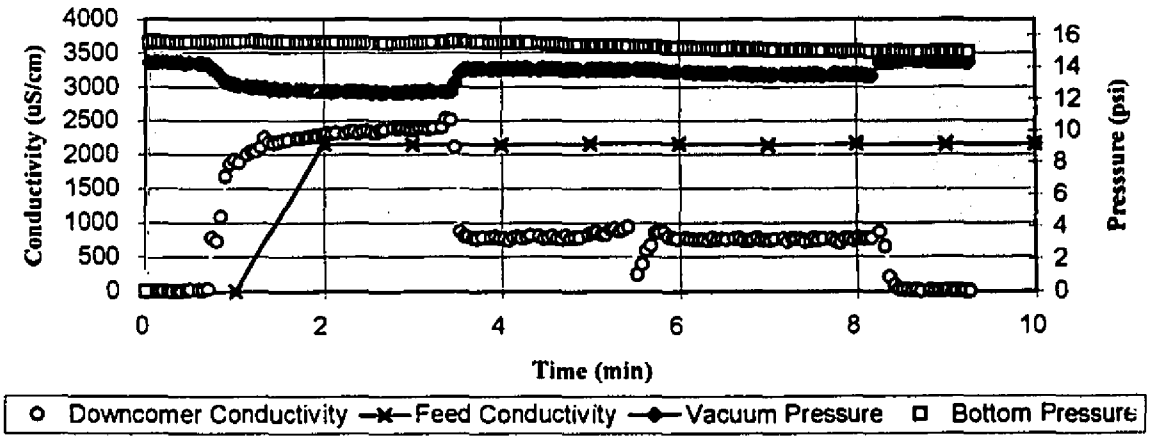

Figure 4.21 Signals taken during a test on secondary copper rougher feed in which a slug passed through the downcomer conductivity cell

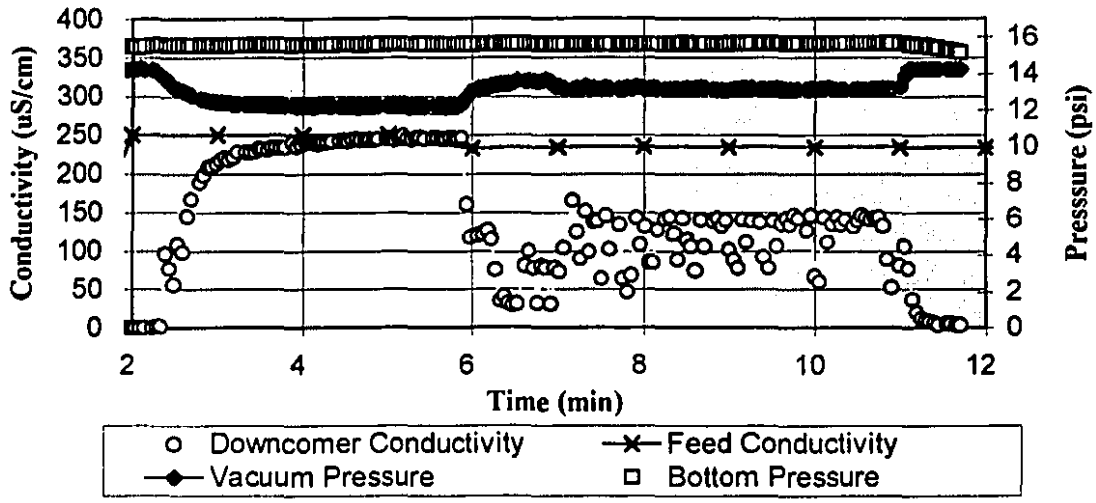

Figure 4.22: Signals taken during a test on final tailings in which slugs passed through the downcomer

CHAPTER 5

INTERACTION BETWEEN THE SEPARATION TANK AND DOWNCOMER IN THE JAMESON CELL

5.0 INTRODUCTION

The downcomer (where particle collection occurs) and the separation tank (where froth/pulp separation occurs) have individual operating parameters that need to be optimized. However, the Jameson cell is similar to a flotation column in that variables in one zone can affect the variables in the other (Finch and Dobby, 1990). The effect of the separation tank level on downcomer behaviour , and downcomer gas flowrate on the separation tank performance was investigated in order to determine the interrelationship between the two zones.

5.1 THE EFFECT OF SEPARATION TANK LEVEL ON DOWNCOMER PERFORMANCE

5.1.1 Experimental Procedure

All experiments were conducted using a water-air, two-phase system. A frother dosage of 10 ppm (Dowfroth 250C) was used, and the Jameson cell was operated with a constant feed flowrate and a variable gas flowrate. Once the system was in equilibrium, as determined by a constant downcomer cell conductivity reading, the separation tank discharge flowrate was adjusted with a variable speed pump so that the top of the froth level was maintained at the lip of the overflow launder. The level in the separation tank was then incrementally lowered until the level reached the end of the downcomer. The data acquisition system provided continuous conductivity and pressure measurements during this process. At

each level (measured from the top of the separation tank (h)), and the pool level in the downcomer (the distance from the top of the downcomer (z)), were measured manually.

5.1.2 Results and Discussion

Two sets of experiments were performed: Set A, where the gas flowrate was allowed to change, and Set B, in which the gas flowrate was maintained constant at the initial, *i.e.*, h = 0, value.

5.1.2.1 Set A

Figures 5.1 and 5.2 display data taken with the Jameson cell operating at a constant feed superficial velocity (with respect to the downcomer) of 10 cm/s and varying the initial gas superficial velocity from 1.68 to 5.06 cm/s. Figure 5.1 shows that the pressure at the top of the downcomer, P_{vac}, decreased as the level in the separation tank decreased. The pool level in the downcomer decreased when the level in the separation tank decreased (Figure 5.2).

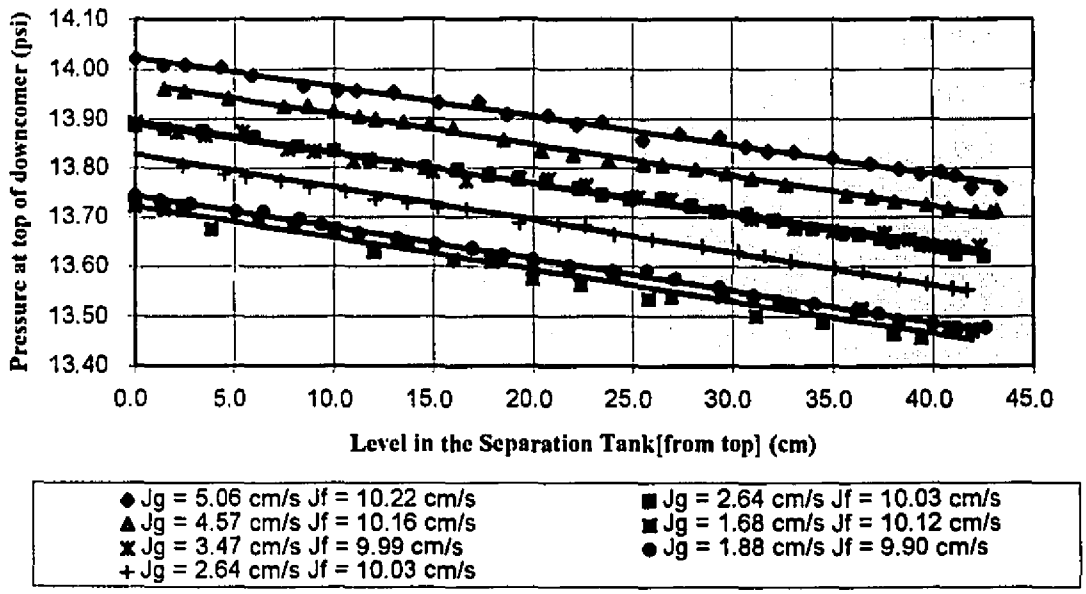

Figure 5.1 Pressure at the top of the downcomer vs. level in the separation tank [Set A]

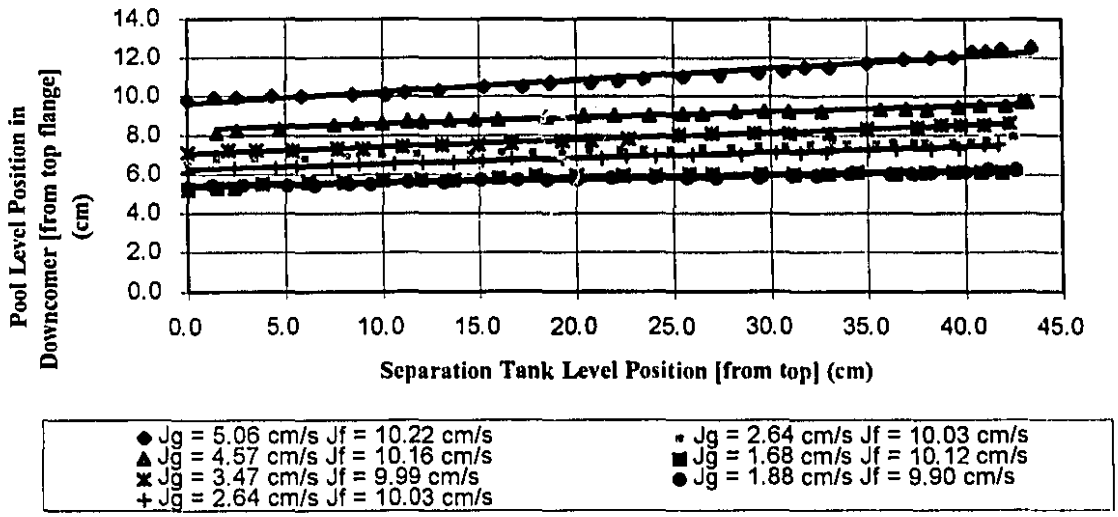

Figure 5.2 Pool level in the downcomer vs. level in the separation tank [Set A]

Figure 5.3 shows that the superficial gas velocity increased as the level in the separation tank decreased. This increase in gas flowrate is due to the increased vacuum at the top of the downcomer, shown in Figure 5.1. It appears that the increase in vacuum caused more air to be aspirated into the downcomer. As a consequence, the vacuum could no longer sustain the level of liquid in the downcomer. A point is reached as the gas flowrate increases where the jet can longer entrain all the air. Consequently, the pool level decreases and thus the free jet length increases, causing the rate of air entrainment by the jet to increase. A new equilibrium pool level is attained where by the jet can entrain all of the aspirated air (Evans *et al.*, 1994). As the gas flowrate increased in the downcomer, with the feed flowrate held constant, the gas holdup showed a corresponding increase as the level in the separation tank decreased (Figure 5.4).

6.1.2.2 Set B

In this set of experiments, the gas flowrate was maintained constant by readjusting it to the initial value, *i.e.*, that when the separation tank was full (h = 0 cm).

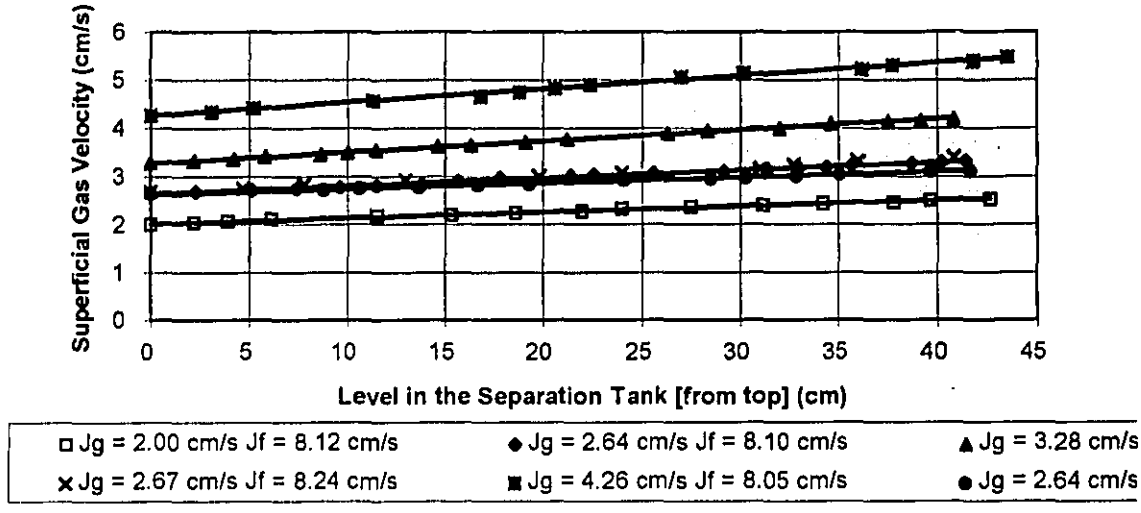

Figure 5.3 Downcomer superficial gas velocity vs. level in the separation tank [Set A]

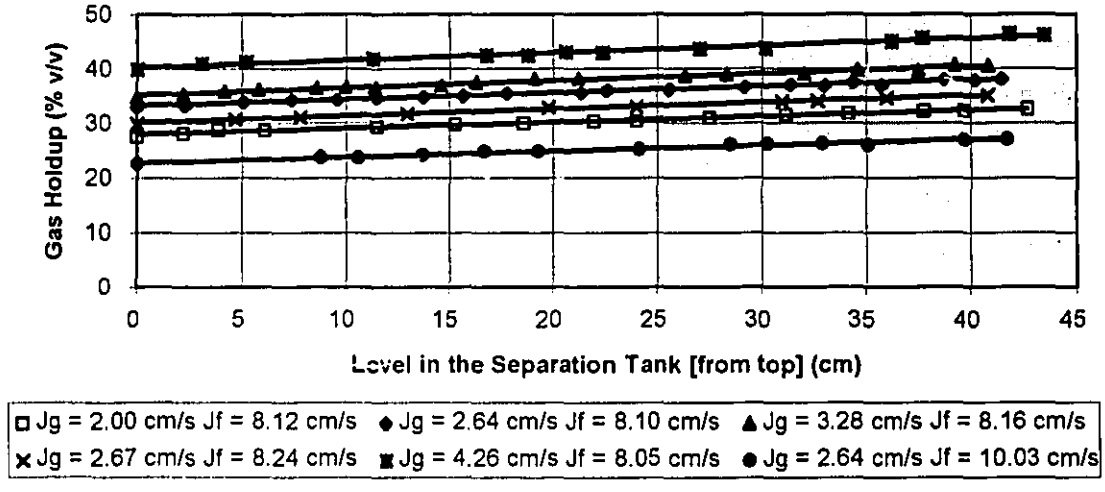

Figure 5.4 Downcomer gas holdup vs. level in the separation tank [Set A]

Figure 5.5 shows that the pressure at the top of the downcomer, P_{vac}, still decreased with decreasing level in the separation tank in a manner similar to that observed in Set A. Thus, whether the gas flowrate was allowed to change or was held constant, it had no effect on the relationship between the vacuum pressure and the separation tank level. Figure 5.6 shows the relationship between level in the downcomer with respect to the level in the separation tank. The level in the downcomer did not change because the air flowrate to the Jameson cell was

held constant. Otherwise, the jet length/pool level relationship would have had to change in order to be able to entrain all of the incoming air.

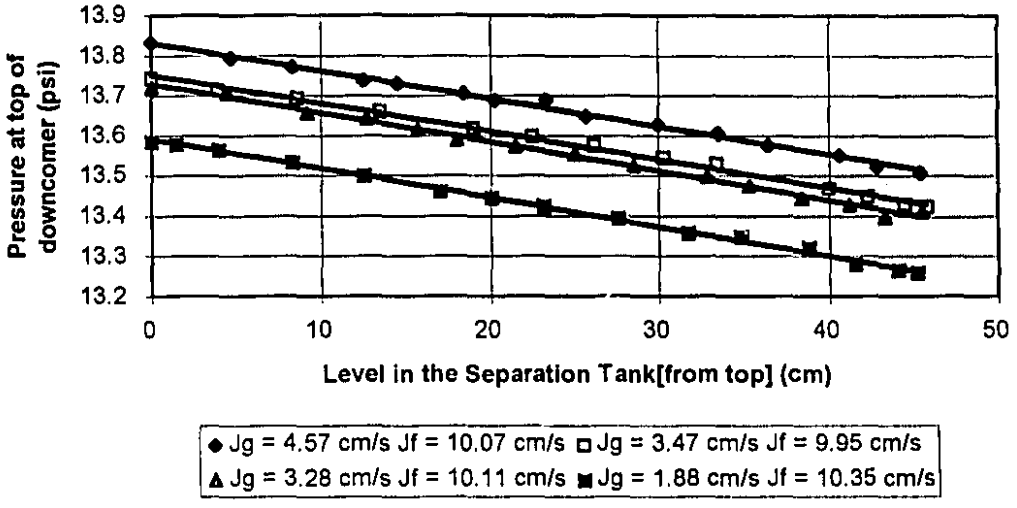

Figure 5.5 Pressure at the top of the downcomer vs. level in the separation tank [Set B]

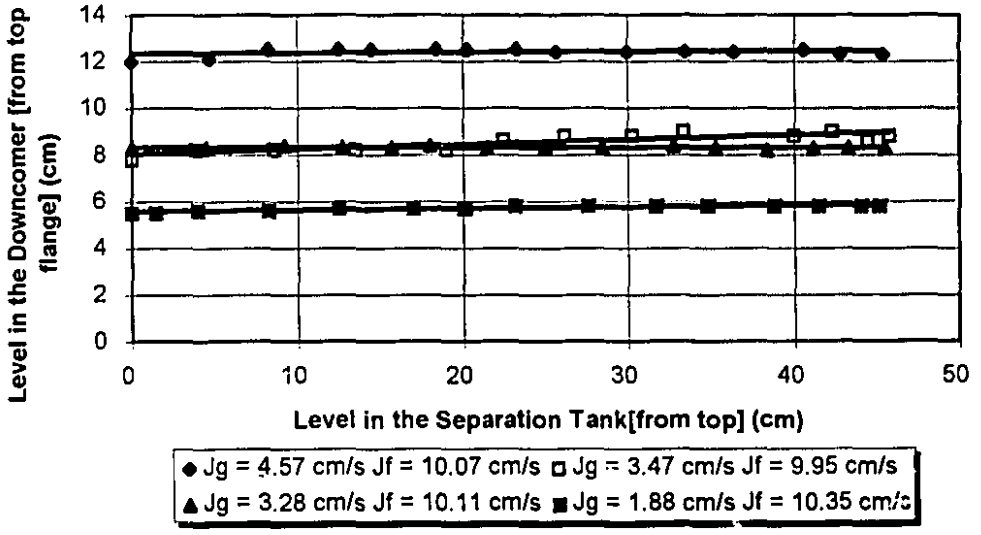

Figure 5.6 Pool level in the downcomer vs. level in the separation tank [Set B]

The pressure at the top of the downcomer has a direct relationship with the head pressure caused by the level of liquid in the separation tank. Figure 5.7 shows that as the

vacuum pressure, P_{vac}, decreased with decreasing pressure at the bottom of the downcomer (measured at the pressure tapping point on the separation tank wall), P_{bot}. This comes from the pressure balance in the system (Equation 5.1):

$$P_{vac} + P_d + P_h = P_{bot} + P_a \qquad (5.1)$$

Where:

P_{vac} is the vacuum pressure at the top of the downcomer

P_d is the dynamic pressure of the liquid jet decelerating into the downcomer pool

P_h is the hydrostatic pressure due to the liquid in the downcomer

P_{bot} is the pressure at the bottom of the dowcomer

P_a is the atmospheric pressure exerted on the liquid in the separation tank

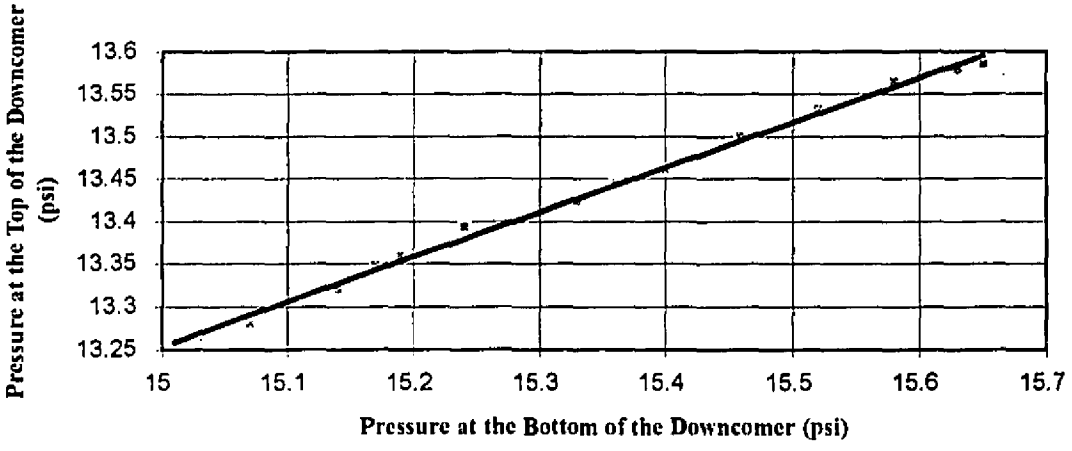

Figure 5.7 Pressure balance in the downcomer

5.2 THE EFFECT OF SEPARATION TANK LEVEL ON MIXING ZONE LENGTH

Experiments were carried out using a stagnation pressure probe with the goal of acquiring a database for hydrodynamic modelling of the downcomer. A prime objective was

to determine whether stagnation pressure measurements could be used to determine the length of the mixing zone, as had previously been demonstrated using static pressure measurements (Evans, 1990).

5.2.1 Experimental Apparatus

The final leg of the experimental work performed at McGill involved an upgrade of instrumentation in order to facilitate data acquisition, as well as incorporating pumps in both the feed and tailings lines that were capable of handling higher flowrates (20-30 l/min).

The feed pump (Lobee, model 700-D-2) is capable of delivering a maximum of 28 l/min to the Jameson cell. The feed is drawn through a 65 L head tank and led through 5.08 cm PVC piping to the top of the downcomer. A 1.91 cm diameter tygon tube is attached to a 5.08 to 1.91 cm reducer, connected to the top of the downcomer. In order to reduce the pressure drop incurred in the previous design of the headspace-nozzle delivery system, which included a 1.27 cm ID inlet which expanded to a 3.81 cm ID headspace then reduced to a 0.63 cm nozzle feed tube, the headspace was eliminated and thus the 1.91 cm feed reduces directly to the 0.63 cm feed tube.

The cell tailings (and overflow) were pumped back to the head tank with the use of a progressing cavity pump (Robin Myers, model 35604) and a globe valve for coarse flowrate control, connected in parallel with a Masterflex peristaltic pump, whose variable pumping speed enabled fine tuning of tailings flowrate, to match that of the feed. This was necessary for control of level in the separation tank.

The feed line included a bypass to the head tank in order to change the feed flowrate. A magnetic flowmeter (Krohne, model IFC080) was used to measure the flowrate of the feed material. The flowrate of air drawn by the plunging jet was measured with a electronic flowmeter (MKS Instruments, model 0558A 050L) and regulated with a needle valve.

Pressure measurements were made with the following devices: A pressure transducer (Omega, model PX304 050A5V) was used to measure the vacuum pressure at the top of the downcomer; a second pressure transducer (Omega, model PX154 025DI) was used to

to determine whether stagnation pressure measurements could be used to determine the length of the mixing zone, as had previously been demonstrated using static pressure measurements (Evans, 1990).

5.2.1 Experimental Apparatus

The final leg of the experimental work performed at McGill involved an upgrade of instrumentation in order to facilitate data acquisition, as well as incorporating pumps in both the feed and tailings lines that were capable of handling higher flowrates (20-30 l/min).

The feed pump (Lobee, model 700-D-2) is capable of delivering a maximum of 28 l/min to the Jameson cell. The feed is drawn through a 65 L head tank and led through 5.08 cm PVC piping to the top of the downcomer. A 1.91 cm diameter tygon tube is attached to a 5.08 to 1.91 cm reducer, connected to the top of the downcomer. In order to reduce the pressure drop incurred in the previous design of the headspace-nozzle delivery system, which included a 1.27 cm ID inlet which expanded to a 3.81 cm ID headspace then reduced to a 0.63 cm nozzle feed tube, the headspace was eliminated and thus the 1.91 cm feed reduces directly to the 0.63 cm feed tube.

The cell tailings (and overflow) were pumped back to the head tank with the use of a progressing cavity pump (Robin Myers, model 35604) and a globe valve for coarse flowrate control, connected in parallel with a Masterflex peristaltic pump, whose variable pumping speed enabled fine tuning of tailings flowrate, to match that of the feed. This was necessary for control of level in the separation tank.

The feed line included a bypass to the head tank in order to change the feed flowrate. A magnetic flowmeter (Krohne, model IFC080) was used to measure the flowrate of the feed material. The flowrate of air drawn by the plunging jet was measured with a electronic flowmeter (MKS Instruments, model 0558A 050L) and regulated with a needle valve.

Pressure measurements were made with the following devices: A pressure transducer (Omega, model PX304 050A5V) was used to measure the vacuum pressure at the top of the downcomer; a second pressure transducer (Omega, model PX154 025DI) was used to

measure the head pressure on the bottom of the downcomer exerted by the liquid in the separation tank A differential pressure transmitter (Bailey, model BCN 24215150) connected by tygon tubing to a "pressure probe", consisting of a 180 cm long section of 5 mm ID steel tubing, and a 50 cm section of 3 mm steel tubing, was used to measure the stagnation pressure in the downcomer. The pressure probe was inserted into the downcomer through the discharge line of the separation tank and was centered in the downcomer with aid of tripod-like attachments (Figure 5.8).

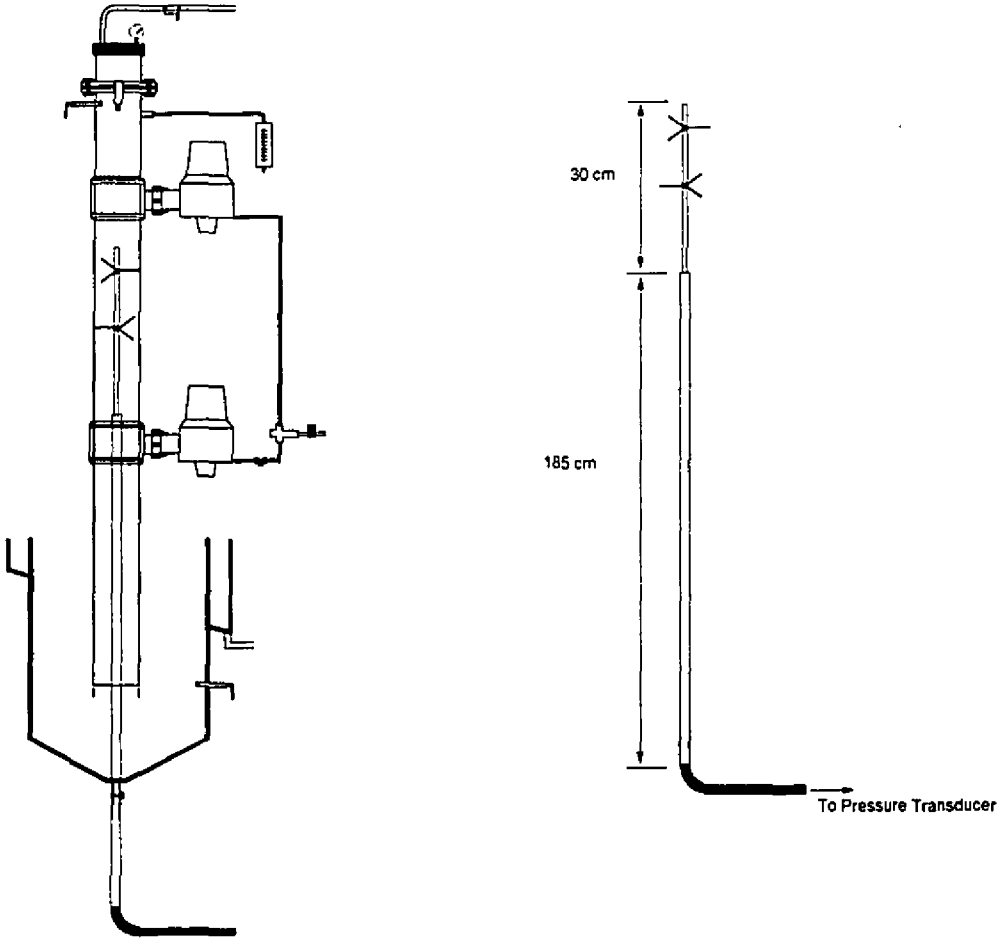

Figure 5.8 Stagnation pressure probe schematic

5.2.2 Experimental Procedure

The gas and liquid flowrates were set at the beginning of each test. The level in the separation tank was then lowered to a certain position. The "new" gas flowrate caused by the change in level in the separation tank was recorded and maintained throughout the remainder of the test. The measurements using the "pressure probe" began at position 0, *i.e.* the bottom of the downcomer, until the top of the pool of liquid in the downcomer was reached. Increments of 10 cm in probe position were used for the first 130 cm, as the pressure readings did not show any change. The position where the stagnation pressure started to rise rapidly was judged as the bottom of the mixing zone. Once the point where the pressure began to rise was reached, smaller increments of probe positioning were used. In the first 3 sets of tests, the tests were stopped once the pressure readings again become constant at a certain position, always at the same maximum pressure. It was found out that a too small scale on the pressure transducer connected to the probe was initially used (0-200" H_2O). The scale was changed to 0-400" H_2O for the fourth set of tests, and a smaller position increment was used (0.5 cm) around the pressure inflection point (P.I.P), assumed to be the beginning of the mixing zone. . The bottom portion of the mixing zone length was determined by the position where the stagnation pressure began to rise, and the length of the mixing zone was calculated by subtracting the position of the stagnation pressure inflection point from the position of the top of the liquid in the downcomer, z, (*i.e.*, mixing zone length = distance between bottom of downcomer and nozzle tip - position of pressure probe tip - free jet length).

5.2.3 Results and Discussion

5.2.3.1 Test 1: (Q_{feed} = 27 l/min, Q_{air} = 30 l/min)

The stagnation pressure readings were taken with the level in the separation tank set to the following positions: h=0, 9.2, 24.4, 32.6, and 38.3 cm, 0 being the position corresponding to the overflow lip (Figure 5.9). The mixing zone length tended to decrease, from 37.6 cm (@ h=0 in sep. tank) to 32.6 cm (@ h=38.3 cm) (Table 5.1).

5.2.2 Experimental Procedure

The gas and liquid flowrates were set at the beginning of each test. The level in the separation tank was then lowered to a certain position. The "new" gas flowrate caused by the change in level in the separation tank was recorded and maintained throughout the remainder of the test. The measurements using the "pressure probe" began at position 0, *i.e.* the bottom of the downcomer, until the top of the pool of liquid in the downcomer was reached. Increments of 10 cm in probe position were used for the first 130 cm, as the pressure readings did not show any change. The position where the stagnation pressure started to rise rapidly was judged as the bottom of the mixing zone. Once the point where the pressure began to rise was reached, smaller increments of probe positioning were used. In the first 3 sets of tests, the tests were stopped once the pressure readings again become constant at a certain position, always at the same maximum pressure. It was found out that a too small scale on the pressure transducer connected to the probe was initially used (0-200" H_2O). The scale was changed to 0-400" H_2O for the fourth set of tests, and a smaller position increment was used (0.5 cm) around the pressure inflection point (P.I.P), assumed to be the beginning of the mixing zone. . The bottom portion of the mixing zone length was determined by the position where the stagnation pressure began to rise, and the length of the mixing zone was calculated by subtracting the position of the stagnation pressure inflection point from the position of the top of the liquid in the downcomer, z, (*i.e.*, mixing zone length = distance between bottom of downcomer and nozzle tip - position of pressure probe tip - free jet length).

5.2.3 Results and Discussion

5.2.3.1 Test 1: (Q_{feed} = 27 l/min, Q_{air} = 30 l/min)

The stagnation pressure readings were taken with the level in the separation tank set to the following positions: h=0, 9.2, 24.4, 32.6, and 38.3 cm, 0 being the position corresponding to the overflow lip (Figure 5.9). The mixing zone length tended to decrease, from 37.6 cm (@ h=0 in sep. tank) to 32.6 cm (@ h=38.3 cm) (Table 5.1).

Table 5.1 Results From Test 1

h, cm	P.I.P., cm	z, cm	M.Z.L., cm	$J_{g,s}$ cm/s
0	132	15.8	37.2	1.60
9.2	130	18.7	36.3	1.63
24.4	130	18.5	36.5	1.67
32.6	132	19.2	33.8	1.71
38.3	132	20.4	32.6	1.70

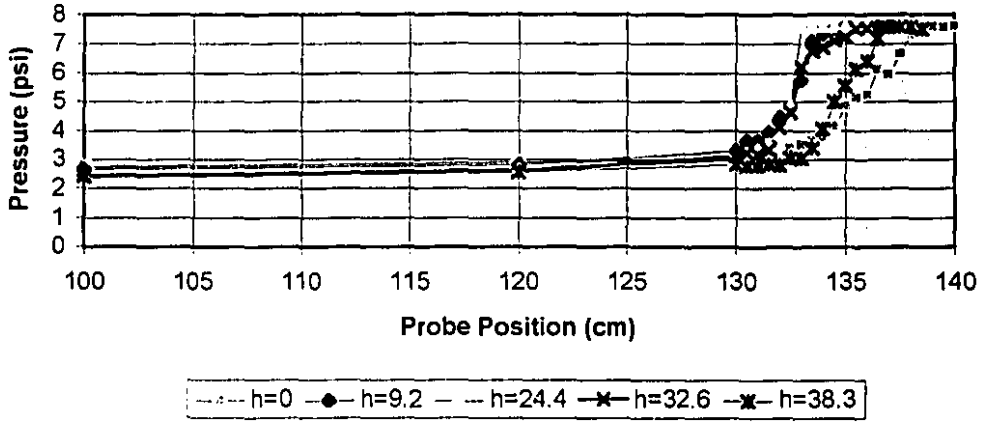

Figure 5.9 Stagnation pressure vs. probe position [Test 1]

5.2.3.2 Test 2: (Q_{feed} = 27.6 l/min, Q_{air} = 25 l/min)

Increments of 2 cm were used when the pressure probe approached the mixing zone, as opposed to Test # 1, where increments of 1 cm were used. The insufficiently small increment probably caused the inconclusive results (Figure 5.10 and Table 5.2).

Table 5.2 Result From Test 2

h, cm	P.I.P., cm	z, cm	M.Z.L., cm	J_g, cm/s
0	142	7.6	35.4	1.33
9.5	140	10.6	34.4	1.35
20.3	138	11.4	35.6	1.39
27.5	140	9.5	35.5	1.40
39	138	10.5	36.5	1.41

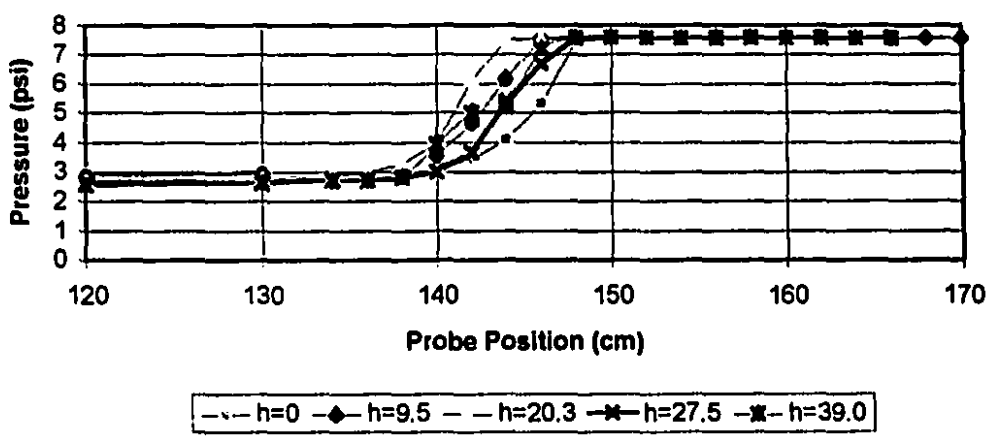

Figure 5.10 Stagnation pressure vs. probe position [Test 2]

5.2.3.3 Test 3: (Q_{feed} = 27.6 l/min, Q_{air} = 15 l/min)

This set of tests was also performed using 2 cm increments of probe position near the beginning of the mixing zone (Figure 5.11). Again, as in test 2, no relationship was determined between the calculated mixing zone length and the level in the separation tank (Table 5.3).

Table 5.2 Result From Test 2

h, cm	P.I.P., cm	z, cm	M.Z.L., cm	J_g, cm/s
0	142	7.6	35.4	1.33
9.5	140	10.6	34.4	1.35
20.3	138	11.4	35.6	1.39
27.5	140	9.5	35.5	1.40
39	138	10.5	36.5	1.41

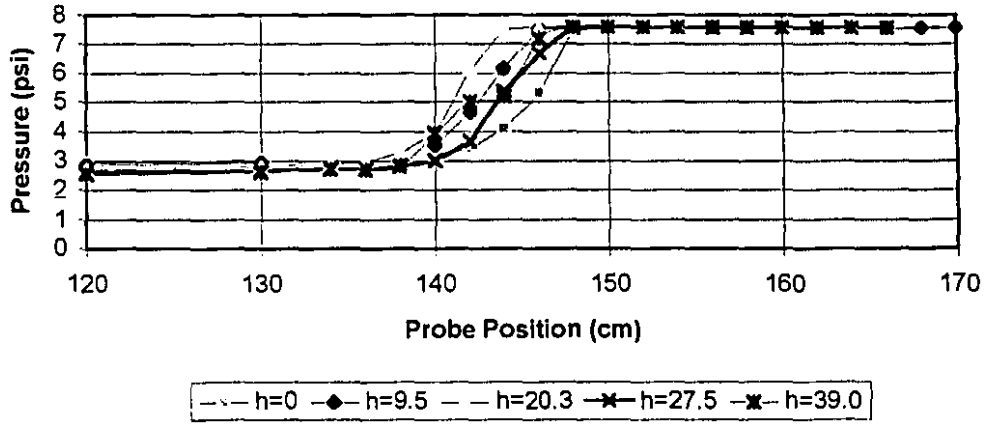

Figure 5.10 Stagnation pressure vs. probe position [Test 2]

5.2.3.3 Test 3: (Q_{feed} = 27.6 l/min, Q_{air} = 15 l/min)

This set of tests was also performed using 2 cm increments of probe position near the beginning of the mixing zone (Figure 5.11). Again, as in test 2, no relationship was determined between the calculated mixing zone length and the level in the separation tank (Table 5.3).

Table 5.3 Results From Test 3

h, cm	P.I.P., cm	z, cm	M.Z.L., cm	J_g, cm/s
0	162	4.6	18.4	0.80
8.7	160	4.6	20.4	0.81
18.0	162	4.6	18.4	0.84
28.8	160	4.7	20.3	0.84
38.0	160	5.0	20.0	0.86

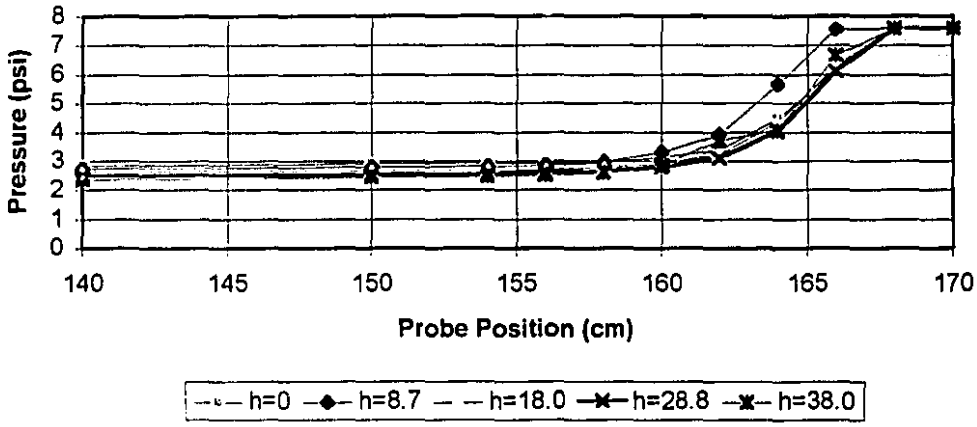

Figure 5.11 Stagnation pressure vs. probe position [Test 3]

5.2.3.4 Test 4: (Q_{feed} = 27.6 l/min, Q_{air} = 15 l/min)

In these tests a probe position increment of 0.5 cm was used to try to determine the bottom of the mixing zone (Figure 5.12). Despite the use of a smaller increment, the pressure measurements again failed to show a consistent relationship between the level in the separation tank and the mixing zone length. Perhaps the pressure probe and the stabilisers that position the probe tip in the centre of the downcomer cause a flow disturbance in the downcomer, which corrupts the data.

Table 5.4 Results From Test 4

h, cm	P.I.P., cm	z, cm	M.Z.L., cm	J_g, cm/s
0	150	6.8	24.6	1.06
9.3	145	7.1	29.3	1.09
23.6	146	7.6	27.8	1.12
31	144	7.6	29.8	1.14
37.2	150	9.3	22.1	1.15

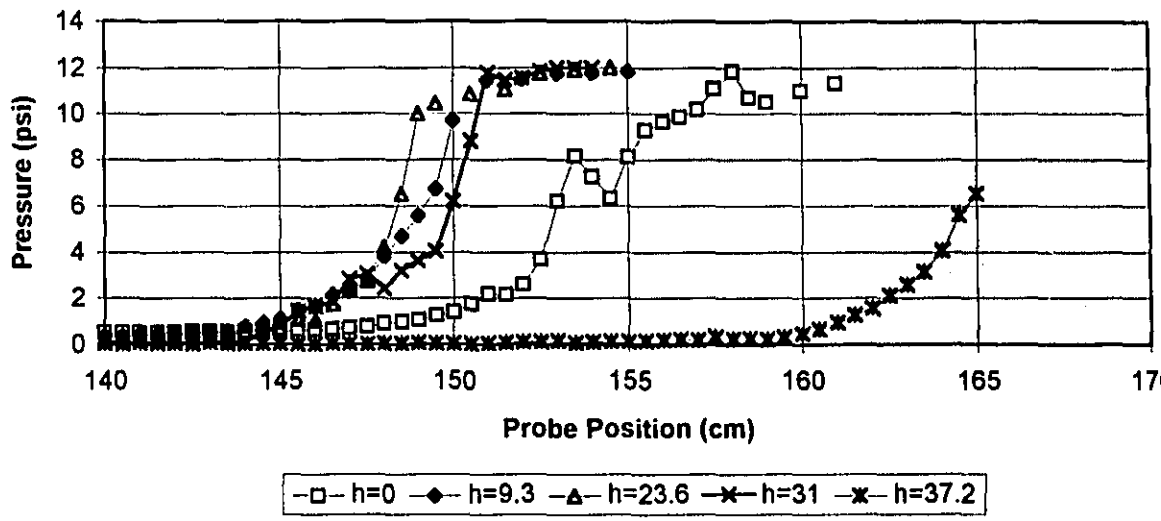

Figure 5.12 Stagnation pressure vs. probe position [Test 4]

According to Evans (1990), the mixing zone length should increase as the gas-to-liquid flow ratio increases. This is because the rate of energy dissipation of the submerged jet decreases as the flow ratio increases, due to the increased density difference across the submerged jet/surrounding liquid boundary. The in turn increases velocities of the recirculating eddies and creates a longer mixing zone. Within each set of tests, the mixing zone length data is quite scattered: Test 1 shows an increase in mixing zone length as the $J_{g,s}$ increases, while Tests 2, 3, and 4 fail to show any meaningful relationship. If the mixing zone lengths obtained at h = 0 cm for the four tests are compared, the mixing zone length does indeed increase as the

gas-to-liquid flow ratio increases. The lack of confirmation of this during the tests was perhaps due to the interference from the pressure probe itself on the operation of the downcomer: The pressure at the top of the downcomer increased by about 0.1 to 0.3 psi as the probe was moved from the bottom of the downcomer to the bottom of the mixing zone; the probe also was observed to disturb flow patterns in the downcomer as the mixing zone was approached. Perhaps experiments conducted in a larger diameter downcomer would reduce this problem.

5.3 THE EFFECT OF DOWNCOMER GAS FLOWRATE ON SEPARATION TANK PERFORMANCE

In these experiments, two regions in the separation tank were apparent: a froth region in which bubbles rose slowly and a diengagement region where bubbles are in turbulent random motion. (Figure 5.13)

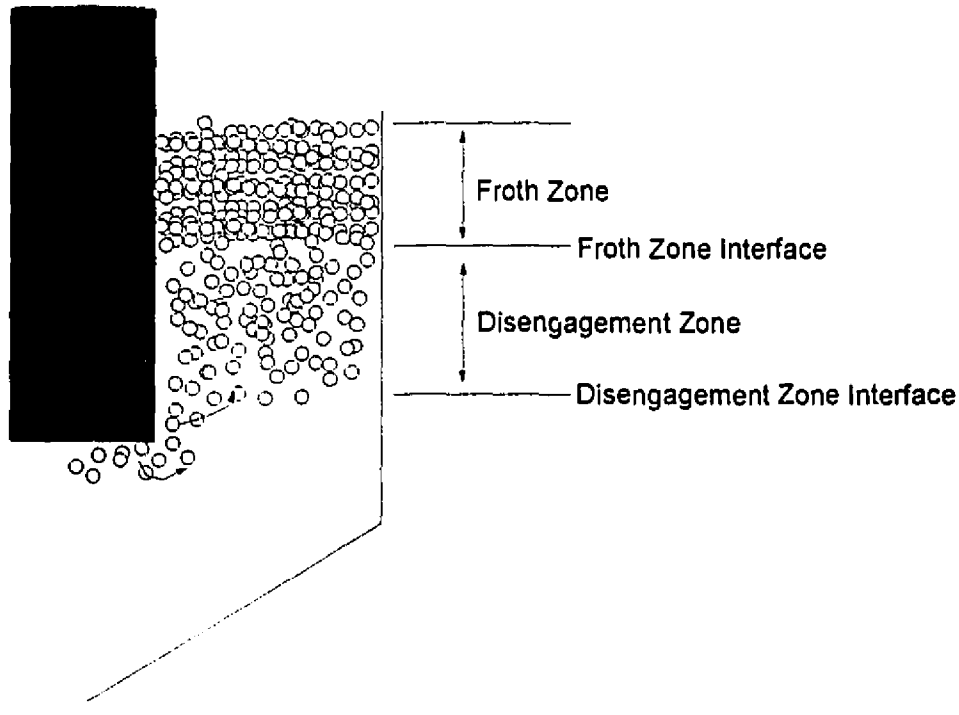

Figure 5.13 Flow Regions of the Separation Tank

The effect of the superficial gas velocity in the separation tank on the characteristics of the disengagement zone and the froth zone were studied. The froth zone interface was defined by a distinct change from a froth zone in which bubbles slowly rose to a turbulent zone below where bubbles swirl in eddies and rise rapidly. The bubbles exiting the downcomer initially cluster around the outer wall due to their low effective density, and then spread laterally in the separation tank as they rise (Evans *et al.*, 1995). The disengagement zone interface position begins at the downcomer discharge and ends at the froth zone interface. The disengagement zone interface position is measured at the point in the separation tank where the bubble-free liquid zone intersects the mass of bubbles discharging from the downcomer.

5.3.1 Experimental Procedure

Two tests were performed with the goal of determining the effect of gas flowrate in the separation tank on the froth zone interface position. In the first test, at a feed flowrate of 27.6 l/min (J_f = 40.12 cm/s in the downcomer) and a frother dosage of 25 ppm (Dowfroth 250C), the air line valve was opened so that 32.8 l/min (48.07 cm/s) of air was drawn by the jet. Thus the initial gas-liquid flow ratio was 1.2. Pressure measurements (vacuum, separation tank) were taken by the data acquisition system, with manual readings of the froth zone interface position (froth depth) and the position of the disengagement zone interface. Two distances were, therefore recorded: from the bubble-free liquid to the bottom of the disengagement region (which is termed the disengagement zone interface) and from this interface to the start of the froth zone (the froth zone interface). The air flowrate was then decreased in increments of approximately 1 l/min (1.46 cm/s). In the second test, the air flowrate was decreased in larger intervals, and the possibility of "losing" the froth zone interface when the air flowrate was returned to a high value was investigated.

5.3.2 Results and Discussion

5.3.2.1 First Test

As stated the ratio of flows in the downcomer, J_g/J_l, was initially set at 1.2. The gas flowrate was diminished by intervals of 1 l/min (1.4 cm/s in the downcomer). No distinct froth

zone interface was observed until the air flowrate was decreased to 26.4 l/min or a J_g^s in the separation tank of 1.44 cm/s (where J_g^s is the superficial gas velocity in the separation tank, and J_g^d is that in the downcomer). The interface position at its initial sighting was 4.3 cm below the overflow lip of the separation tank. Unfortunately, due to the design of the overflow launder, a clear view the top 14 cm of the separation tank is obscured. At the end of the test, when the air was turned off, water was overflowing in the separation tank indicating that the liquid level, or specifically the tailings flowrate was not well controlled, thus resulting in a decreasing froth depth as the test progressed. As shown in Figure 5.14, the decrease in froth depth does correspond to further decrease in superficial gas velocity in the separation tank. This relationship, however, may be due to the lack of tailings flowrate control. It should be noted from the figure that at low gas rates the disengagement zone interface lies above the bottom of the downcomer. Figure 5.15 shows the increase in hydrostatic pressure in the separation tank as the superficial gas velocity was reduced and the effective level of water in the separation tank increased. The pressure signal increased by 0.116 psi as J_g^s decreased from 1.44 to 0.68, or a corresponding increase of 8.2 cm head of water pressure. Therefore in this portion of the test, the equivalent water level increased by 8 cm, while the actual interface was observed to increase by 4.3 cm. It is difficult to determine whether the gas flowrate decrease or the level increase caused the interface position change (probably a combination of both). Indeed, these findings indicate that perhaps the level may be calculable using pressure signals.

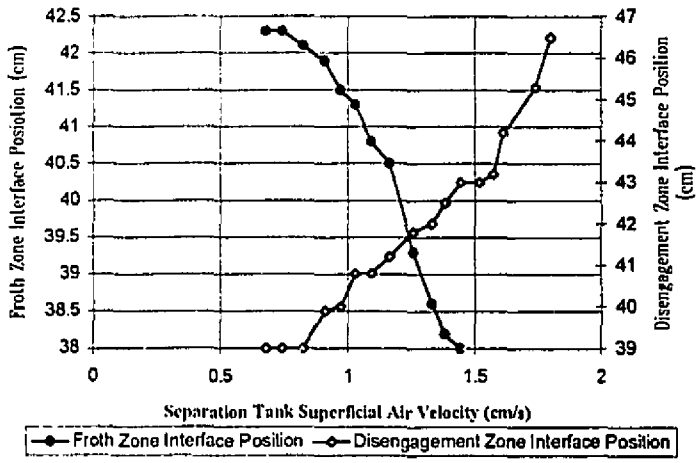

Figure 5.14 Froth and disengagement zone interfacial position vs. superficial air velocity

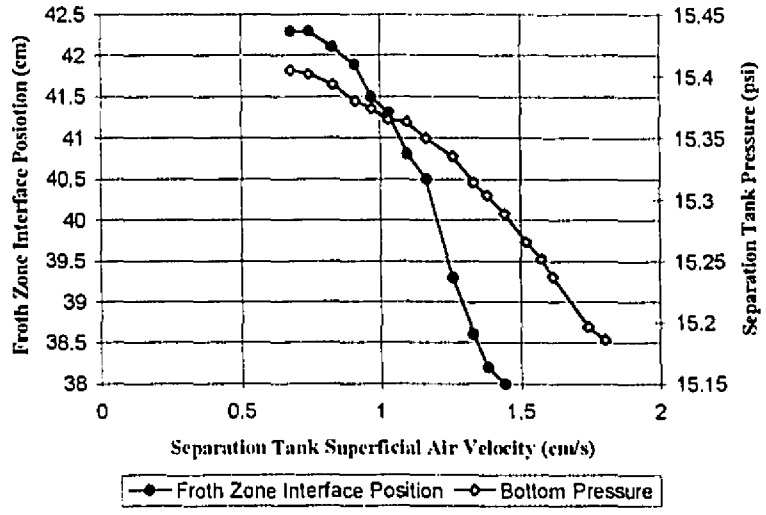

Figure 5.15 Froth zone interface position and separation tank pressure vs. superficial air velocity

Figure 5.16 demonstrates that the vacuum pressure in the downcomer, shown in previous work to vary directly with the separation tank pressure, decreases as the separation tank pressure increases. The vacuum pressure is therefore governed by the change in gas flowrate aspirated the downcomer.

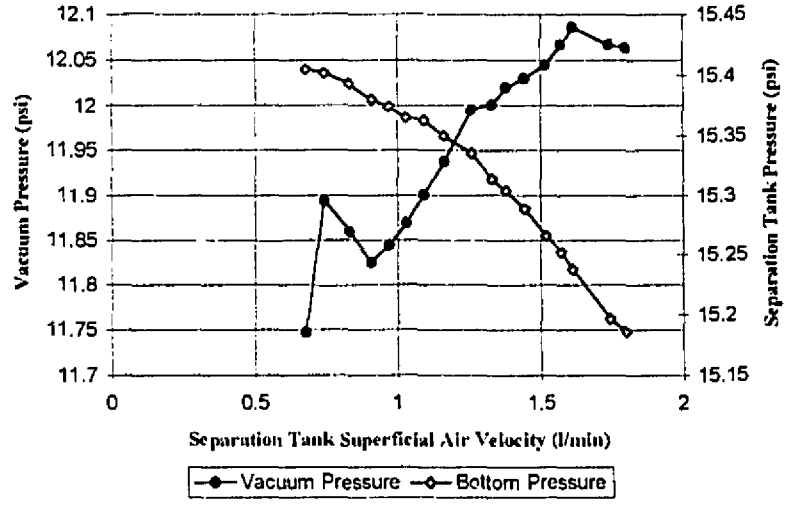

Figure 5.16 Vacuum and separation tank pressure vs. superficial air velocity

6.3.2.2 Second Test

In this test, the level of liquid in the separation tank, prior to allowing gas into the downcomer, was lowered to a position approximately 30 cm below the overflow launder lip to ensure that the interface could be observed in the lower portion of the separation tank. No interface was detected at the highest gas flowrate 32.69 l/min (J_g^s = 1.79 cm/s); however, at the two following gas settings 30.52 and 27.91 l/min an interface was observed. This was not a distinct flat interface but a point where the change from the turbulent conditions to quiescent characteristic of the froth zone was judged to have occured. At the fourth flowrate, 25.51 l/min (J_g^s = 1.40 cm/s), a distinct interface was observed. From Figure 5.17, it is shown that as the gas flowrate is initially decreased trends in the position of the and disengagement zone interfaces are opposite.

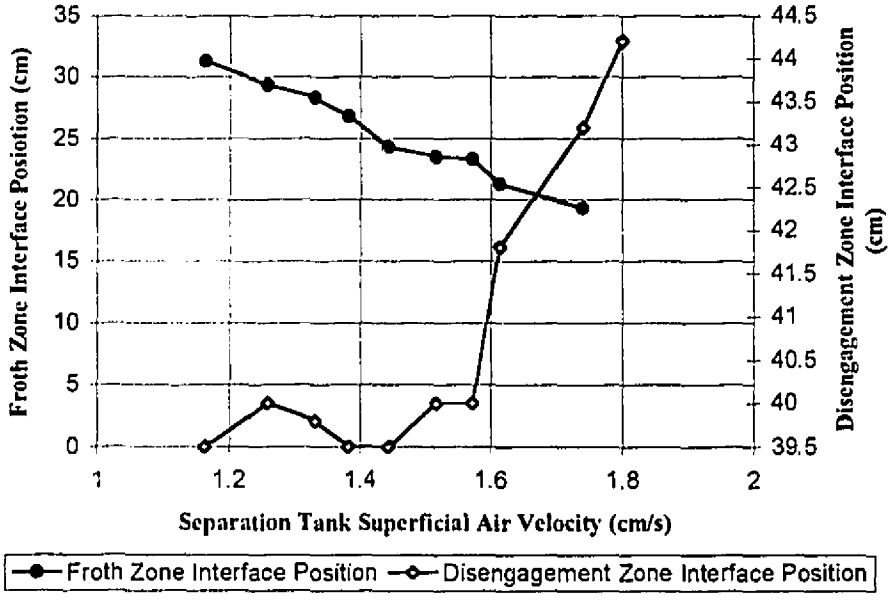

Figure 5.17 Froth and disengagement zone interface positions vs. superficial air velocity

Then as the gas flowrate is increased to the original value, the froth zone interface continues to rise (position of interface with respect to overflow lip) while the disengagement zone position

is steady. Again, the trend for the froth zone is probably due to the inability to maintain a tailings flowrate equal to that of the feed. In Figure 5.18, the froth zone interface position and separation tank pressure vs. J_g requires close attention to interpret. As the J_g^s is decreased from 1.67 to 1.0 cm/s, the pressure change equals 0.043 psi = 3.02 cm water, while the interface position increased by 8 cm. Subsequently, when the gas flowrate is increased (from 1.0 to 1.72 cm/s), the pressure change is equivalent to 4.6 cm water while the interface position change was 7 cm. So, contrary to the results in Test 1, the change in froth zone interface position has definitely changed due to a change in superficial velocity. Admittedly lack of the tailing flowrate control partly accounted for the change in position, but the interface change is smaller than the level of liquid change. The gas flowrate must have had an effect. Figure 5.19 demonstrates that the vacuum pressure is governed by gas flowrate rather than separation tank pressure.

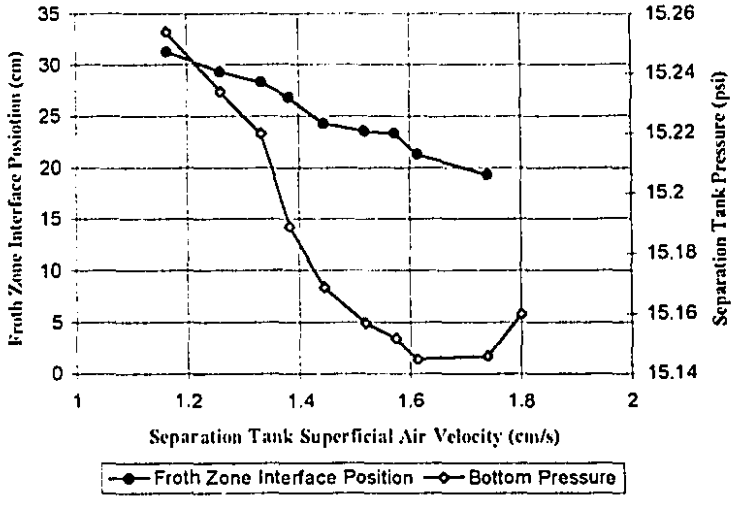

Figure 5.18 Froth zone interface position and separation tank pressure vs. Superficial air velocity

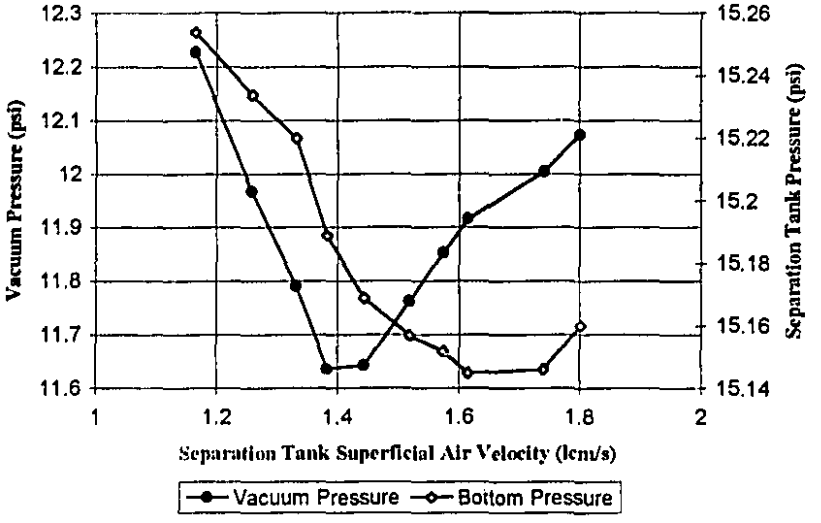

Figure 5.19 Vacuum and separation tank pressure vs. superficial air velocity

CHAPTER 6

CONCLUSIONS AND RECOMMENDATIONS

The effect and interaction of several operating variables on the performance of the Jameson cell was investigated in this thesis.

Ring electrodes, in combination with the Maxwell model, were found to give adequate on-line estimates of gas holdup in the downcomer. Laboratory two-phase tests and in-plant three phase tests showed that the conductivity technique gave reasonable estimations over a gas holdup range of 10-50%, *i.e.*, the normal operating range for the Jameson cell. The conductivity signal also indicated the transition from bubbly flow to slug flow in the downcomer. The application of the ring electrodes in the Jameson cell is promising; however, it has to be established whether the technology can be transferred to industrial use.

The level in the separation tank was found to affect several operating variables of the downcomer. As the level in the separation tank decreased, if the air flowrate was left uncontrolled, the air flowrate increased from its original value. This increase is due to a decrease in pool level causing the free jet length to increase and consequently allowing more air to be entrained in the downcomer. As the level in the separation tank decreases, the head pressure on the bottom of the downcomer decreases causing the pressure at the top of the downcomer to decrease, in order to respect the pressure balance. This decrease in pressure at the top of the downcomer, *i.e.*, increase in vacuum, causes more air to be aspirated into the downcomer. A new equilibrium pool level is reached where the rate of entrainment of air by the jet equals the air flowrate aspirated into the downcomer. When the gas flowrate was held constant at the initial value, the pool level remained constant as the level in the separation tank decreased. The decrease in separation tank level did decrease the pressure at the top of the downcomer. The impetus for this work was

because the personnel at the Kidd Creek concentrator found that changes in level caused changes in Jameson cell performance. The effect of the separation tank level on overall performance would be minimized if good control of the air flowrate was applied (This is generally not the case in practice).

Experiments with the stagnation pressure probe were intended to determine if the mixing zone length changed upon changes in separation tank level. The results were inconclusive. The mixing zone lengths for all of the tests at h = 0 cm did increase with increasing gas-to-liquid flow ratio, but this was the only consistent finding. Further work on these lines may consider using static pressure measurements along the downcomer wall in order to determine mixing zone length. Another alternative to the stagnation pressure probe is the use of multiple ring electrodes to measure conductivity along the downcomer. With proper attention to ring placement the mixing zone length in the downcomer could potentially be determined.

There were mixed results in the tests to determine the effect of the air superficial velocity on froth characteristics. No froth zone interface was observed for $J_g^s \geq 1.44$ cm/s. Above this value, froth flooding occurs and no interface is visible. In one of the two tests an increase in J_g^s did give rise to an increase in froth zone interface level. Both tests were performed with insufficient control of the tailings flowrate, preventing any definite conclusions to drawn from the tests. Further work should be carried out to determine the relationship between the superficial gas velocity in the separation tank on froth zone behaviour. Emphasis should be placed on tailings flowrate control, using a combination of a flowmeter and a variable-speed pump. Conductivity techniques that have been shown to be effective in the measurement of froth depth in mechanical flotation cells and flotation columns could also aid in the tracking of the froth zone interface.

REFERENCES

Atkinson, B. W., and Chatiar, R., 1992. "Void Fraction/Conductivity Relationship - Jameson Cell Downcomer ", Private Communication.

Atkinson, B. W., Griffin, P. T., Jameson, G. J., and Espinosa-Gomez, R., 1993. "Jameson Cell Test Work on Copper Streams in the Copper Concentrator of Mount Isa Mines Limited", presented at the *XVIII International Mineral Processing Congress*, *AusIMM*, 23-28 May, 1993.

Banisi, S., 1994, Ph.D. Thesis, McGill University, Montreal, Canada.

Banisi, S., Finch, J.A., and Laplante, A.R., 1993. "Electrical Conductivity of Dispersions: A Review", *Minerals Eng.*, Vol. 6, No. 4, pp. 369-385.

Begovich, J. M., and Watson, J. S., 1978. "An Electroconductivity Technique for the Measurement of Axial Variation of Holdups in Three-Phase Fluidized Beds", *AIChE Journal*, Vol. 24, No. 2, pp. 351-354.

Blok, J R., and Drinkenburg, A. A. H., 1982. "Hydrodynamic Properties of Pulses in Two-Phase Downflow Operated Packed Columns", *Chem. Eng. J.*, Vol. 25, pp. 89-99.

Bober, W., and Kenyon, R. A., 1980. ''Fluid Mechanics'', New York: John Wiley & Sons, 1980.

Braunstein, J., Robbins, G. D., 1971. "Electrolytic Conductance Measurements and Capacitive Balance", *J. Chem. Ed.*, Vol., No. 1, pp. 52-59.

Cole, R. H., and Coles, J. S., 1964, *Physical Principles of Chemistry*, W. H. Freeman and Company, 795 pp.

De La Rue, R. E., and Tobias, C. W., 1959. "On the Conductivity of Dispersions", *J. Electrochemical Soc.*, Vol. 106, No. 9, pp. 827-833.

Evans, G. M., 1990. "A Study of a Plunging Jet Bubble Column", Ph.D. Thesis, University of Newcastle, New South Wales, Australia.

Espinosa-Gomez, R., Johnson, N. W., Pease, J. D., and Munroe, P.D., 1989. "Commissioning of the First Flotation Columns at Mount Isa Mines Limited ", *Processing of Complex Ores*, Proceedings of an International Symposium (Eds: G. S. Dobby, and S. R. Rao), Halifax, Canada, Permagon Press: New York, pp. 311-324.

G. M., Jameson, G. J., and Atkinson, B. W., 1992. "Prediction of the Bubble Size Generated by a Plunging Liquid Jet Bubble Column", *Chem. Eng. Sci.*, Vol. 47, No. 13/14, pp. 3265-3272.

Evans, G. M., Jameson, G. J., and Atkinson, B. W., 1994. "The Jameson Cell ", *from Flotation Science and Engineering* (Ed: K. A. Matis), Marcel Dekker Inc., Ch. 12, pp. 331-363.

Evans, G. M., Jameson, G. J., and Reilly, C. D., 1994. "Free Jet Expansion and Gas Entrainment Characteristics of a Plunging Liquid Jet", Presented at the *International Colloquium on Jets, Wakes and Shear Layers*, Melbourne, Australia, 18-20 April, 1994.

Finch, J. A. and Dobby, G. S., 1990. *Column Flotation*, Permagon Press: Oxford, 180 pp.

Finch, J. A., Uribe-Salas, A., and Xu, M., 1995. "Column Flotation ", in *Flotation Science and Engineering* (Ed: K. A. Matis), Marcel Dekker Inc., New York., Ch. 11.

Finch, J.A., 1993. Private Communication.

Harbort, G. J., Jackson, B. R., and Manlapig, E. V., 1994. "Recent Advances in Jameson Flotation Cell Technology ", *Minerals Engineering*, Vol. 7, Nos 2/3, pp. 319-332.

Huls, B. J., Lachance, C. D., and G. S. Dobby, 1989. "Gas Rate and Froth Depth Effects on Performance of a Cu-Ni Separation Flotation Column", *Processing of Complex Ores: Proceedings of an International Symposium* (Eds.: G. S. Dobby, and S. R. Rao), Halifax, Nova Scotia, Canada, Aug. 20-24, Permagon Press, New York, pp. 311-324.

Jameson, G. J. and Manlapig, E. V., 1991. "Applications of the Jameson Flotation Cell", *COLUMN '91*, Proc. Int. Conf. Column Flotation, (G. Agar, B. Huls, D. Hyma Eds.), Sudbury, Ontario, June 2-6, Vol. 2, pp. 673-687.

Jameson, G. J. and Manlapig, E. V., 1991. "Flotation Cell Design-Experiences with the Jameson cell", *Proc. AUSIMM Extractive Metallurgy Conference*, October 1991, pp. 1-6.

Jameson, G. J., 1988. "A New Concept in Flotation Column Design", *Column Flotation '88 Proceedings* (Ed. K.V.S. Sastry), Phoenix, Arizona, pp. 281-285.

Marchese, M. M. , 1991. "Hydrodynamic study of a downwards concurrent bubble column", Master's Thesis, McGill University, Montreal, Canada.

Marchese, M. M. , 1993. Private Communication

Marchese, M. M. , Uribe-Salas, A., and Finch, J. A.. 1992. "Measurement of Gas Holdup in a Three-Phase Concurrent Downflow Column" , *Chem. Eng. Sci.*, Vol. 47, No. 13/14, pp. 3475-3482.

Marchese, M. M., Uribe-Salas, A., and Finch J. A., 1993. "Hydrodynamics of a Downflow Column", *XVIII International Mineral Processing Congress, AusIMM*, 23-28 May, 1993, pp. 813-822.

Maxwell, J. C. 1892. *A Treatise in Electricity and Magnetism*, 3rd Ed., Vol. 1, Pt. II, Ch. IX, pp. 435-449, (Oxford University Press: London)

Nasr-El-Din, H., Shook, C. A., and Colwell, J., 1987. "A Conductivity Probe for Measuring Local Concentrations in Slurry Systems", *Int. J. Multiphase Flow*, Vol. 13, No. 3, pp. 365-378.

Oshinowo, T., and Charles, M. E., 1974. "Vertical Two-Phase Flow - Part I. Flow Pattern Correlations", *Can. J. Chem. Eng.*, Vol. 52, pp. 25-35.

Probst, A., Xu, M., and Finch, J. A., 1992. "Interface Level Detection Using Conductivity in the Separation Compartment of a Jameson Cell", Internal Report, McGill University.

Sawyer, D. T., and Roberts, J. L., 1974. *Experimental Electrochemistry for Chemists*, John Wiley & Sons, Inc., 435 pp.

Shah, Y. T., Kulkarni, A. A., Wieland, J. H., and Carr, N. L., 1983. "Gas Holdup in Two and Three-Phase Downflow Bubble Columns", *Chem. Eng. J.*, 26, pp. 95-104.

Tremblay, R., Roberts, K., and Burrows, M., 1993. "Jameson Cell Testing at the Kidd Creek Concentrator", *Proceedingd 25th Annual CMP Meeting*, Jan. 19-21, 1993, Paper 23.

Tsochatzidis, N. A., Karapantsios, T. D., Kostoglou, M. V., and Karabelas A. J., 1992. "A Conductance Probe for Measuring Liquid Fraction in Pipes and Packed Beds", *Int. J. Multiphase Flow*, Vol. 18, No. 5, pp. 653-667.

Turner, J. C. R., 1975. "The Electrical Conductance of Liquid-Fluidized Beds of Spheres", *Chem. Eng. Sci.*, Vol. 31, pp. 487-492.

Uribe-Salas, A., 1991. "Process Measurements in Flotation Columns using Electrical Conductivity", Ph.D. Thesis, McGill University, Montreal, Canada.

Xu, M., Probst, A., and Finch, J. A., 1993. " Level and Solids Profile Detection in Thickeners using Conductivity", Proc. 25th Annual CMP Meeting, Jan. 19-21, 1993, Paper 17.

Yamagiwa, K., Kusabiriaki, D., and Ohkawa, A., 1990. " Gas Holdup and Gas Entrainment Rate in Downflow Bubble Column with Gas Entrainment by a Liquid Jet Operating at High Liquid Throughput", *J. Chem. Eng. Japan*, Vol. 23, No. 3, pp. 343-348.

Yianatos, J. B., Laplante, A. R., and Finch, J. A., 1985. "Estimation of Local Holdup in the Bubbling and Froth Zones of a Gas-Liquid Column", *Chem. Eng. Sci.*, Vol. 40, No. 10, pp.1965-1968.